# Comprehensive assessment of the corrosion inhibition properties of quinazoline derivatives on mild steel in 1.0 M HCl solution: An electrochemical, surface analysis, and computational study

Zakia Aribou, Moussa Ouakki, Fatima El Hajri, Elhachmia Ech-Chihbi, Issam Saber, Zakaria Benzekri, Said Boukhris, Mohammad K. Al-Sadoon, Mouhsine Galai, Charafeddine Jama, et al.

## HAL Id: hal-04905186
### https://hal.univ-lille.fr/hal-04905186v1

Submitted on 22 Jan 2025

# Comprehensive assessment of the corrosion inhibition properties of quinazoline derivatives on mild steel in 1.0 M HCl solution: An electrochemical, surface analysis, and computational study

Zakia Aribou [a], Moussa Ouakki [b,c,*], Fatima El Hajri [b], Elhachmia Ech-chihbi [d], Issam Saber [b], Zakaria Benzekri [b,e], Said Boukhris [b], Mohammad K. Al-Sadoon [f], Mouhsine Galai [a,**], Jama Charafeddine [g], Mohamed Ebn Touhami [a]

[a] Laboratory of Advanced Materials and Process Engineering, Faculty of Sciences, University Ibn Tofail, Kenitra PB. 133-14000, Morocco
[b] Laboratory of Organic Chemistry, Catalysis and Environment, Faculty of Sciences, Ibn Tofaïl University, PO Box 133, Kenitra 14000, Morocco
[c] National Higher School of Chemistry (NHSC), University Ibn Tofail, Kenitra BP. 133-14000, Morocco
[d] Euro-Mediterranean University of Fes, Fez, Morocco
[e] Laboratory of Heterocyclic Organic Chemistry, Department of Chemistry, Faculty of Sciences, Mohammed V University in Rabat, Rabat BP 1014, Morocco
[f] Department of Zoology, College of Science, King Saud University, P.O. Box 2455, Riyadh 11451, Saudi Arabia
[g] University of Lille, CNRS, INRAE, Centrale Lille, UMR 8207, UMET—Unité Matériaux et Transformations, Lille F-59000, France

## ARTICLE INFO

## ABSTRACT

The efficacy of two compounds, namely 12-(4-chlorophenyl)-3,3-dimethyl-3,4,5,12-tetrahydrobenzo[4,5] imidazo[2,1-*b*]quinazolin-1(2H)-one (Q-Cl) and 3,3-dimethyl-12-phenyl-3,4,5,12-tetrahydrobenzo[4,5]imidazo[2,1-*b*]quinazolin-1(2H)-one (Q-H), in inhibiting corrosion on mild steel in 1.0 M hydrochloric acid was evaluated. Surface analytical techniques and electrochemical procedures were employed for examination. The results demonstrated that both Q-Cl and Q-H significantly inhibit corrosion. Specifically, Q-Cl achieved an inhibition efficiency of 85.2 % at a concentration of $10^{-3}$ M, while Q-H exhibited a higher inhibition efficiency of 91.5 %. Electrochemical investigations suggested that both Q-Cl and Q-H acted as inhibitors of mixed-type corrosion. These chemicals efficiently prevented metal corrosion through adsorption, conforming to Langmuir's adsorption isotherm model. The adsorption mechanism of corrosion inhibition was further supported by surface investigations and scanning electron microscopy-energy-dispersive X-ray spectroscopy (SEM-EDX). Additionally, Density Functional Theory (DFT) and other computational approaches were employed to study the anti-corrosion mechanism of Q-Cl and Q-H. These simulations yielded theoretical results that aligned with the preceding experimental findings.

## 1. Introduction

Each year, corrosion has significant global consequences by causing the spontaneous destruction of metallic materials through chemical, biological, and electrochemical interactions with the surrounding environment [1,2]. This phenomenon dramatically influences several industries, leading to potential pollution risks, the need for replacement of corroded parts, or even production stoppages, resulting in substantial economic costs. The frequent application of acid solutions in thermal or chemical treatments of materials [3,4], such as pickling and cleaning of boilers and oil wells, as well as the use of saline solutions as coolants in certain sectors, often leads to significant corrosion issues that require prompt intervention.

To solve this problem, many protection techniques have been developed. Among the most widely used techniques are cathodic protection, treatment with metallic and polymeric coatings, and modification of the corrosive environment [5,6]. The latter strategy is frequently employed by industries and researchers. It involves injecting small

---

quantities of corrosion inhibitors into the aggressive environment. These compounds, known as 'corrosion inhibitors,' must be environmentally safe, cost-effective, and easy to use [7]. Their presence delays or even prevents the dissolution reaction between the substance and its environment.

Organic compounds have been widely recognized for their effectiveness as corrosion inhibitors in industrial applications [8]. These compounds typically contain a variety of functional groups and heteroatoms, such as oxygen, nitrogen, phosphorus, and sulfur, which enable them to adsorb onto metal surfaces. This adsorption forms a protective barrier between the metal surface and the corrosive environment. Moreover, these inhibitors can effectively reduce corrosion by blocking active sites on the metal surface [9–12]. Research indicates that the inhibition efficiency of compounds containing heteroatoms generally follows the order O < N < S < P, which can be attributed to the electronegativity of these atoms [13,14]. It is well-documented that the corrosion inhibition process is primarily due to the formation of donor-acceptor complexes on the iron surface and the electron-donating ability of organic inhibitors [15,16]. Among various nitrogen-containing compounds, Quinazoline Derivatives have been particularly noted for their high efficacy in reducing corrosion rates and preventing hydrogen embrittlement in steels exposed to acidic environments [17,18].

The purpose of the study is to investigate how mild steel is protected in 1.0 M HCl solution by examining the interactions of two distinct organic molecules with the substrate: 12-(4-chlorophenyl)-3,3-dimethyl-3,4,5,12-tetrahydrobenzo[4,5]imidazo[2,1-b]quinazolin-1 (2H)-one and 3,3-dimethyl-12-phenyl-3,4,5,12-tetrahydrobenzo[4,5] imidazo[2,1-b]quinazolin-1(2H)-one. The inhibitory effects of these compounds were compared using stationary and transient electrochemical methods. Complementary techniques, such as surface analysis (SEM-EDAX) and solution analysis (ICP), were employed to provide further insights into the inhibitory mechanism. However, these experimental methods alone do not fully elucidate the mechanisms of action of the inhibitors. To assess the relationship between the inhibitory effects of the investigated derivatives and their molecular structures, Density Functional Theory (DFT) simulations were conducted.

## 2. Experimental details

### 2.1. Materials and sample preparation

The studies are performed on plain steel samples whose chemical composition (%) is shown in Table 1:

The steel substrate underwent a process of sequential polishing using emery paper with different grit sizes, which ranged from 180 to 2000. The samples were then cleaned with distilled water and ethanol and dried at room temperature.

### 2.2. Preparation of solutions

Analytical-grade hydrochloric acid (37 % w/w) was diluted with distilled water to prepare a 1.0 M hydrochloric acid solution, which served as the corrosive medium for the experiments. It is recognized that this solution will damage the steel's surface. The study employed quinazoline derivatives as inhibitors, with concentrations ranging from $10^{-6}$ M to $10^{-3}$ M. The solubility of the inhibitors in the corrosive medium was investigated, and based on that, the aforementioned concentration range was selected. Additionally, a blank solution was prepared for comparison purposes. Table 2 displays the molecular structures of Q-Cl and Q-H, as shown below.
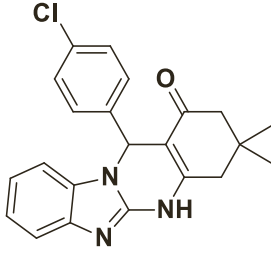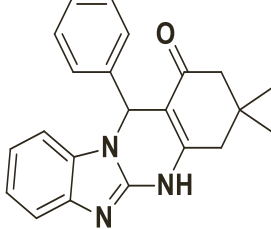
**Table 2**
Noms, structures chimiques et abréviations des composés de pyrane étudiés.

| Abbreviation | Chemical structure | Name / Molar mass |
|---|---|---|
| Q-Cl |  | 12-(4-chlorophenyl)−3,3-dimethyl−3,4,5,12-tetrahydrobenzo[4,5]imidazo[2,1-*b*]quinazolin−1(2H)-one **M=377 g/mol** |
| Q-H |  | 3,3-dimethyl−12-phenyl−3,4,5,12-tetrahydrobenzo[4,5]imidazo[2,1-*b*]quinazolin−1(2H)-one **M=343 g/mol** |

### 2.3. Electrochemical cell

The investigation utilized electrochemical methods, including potentiodynamic polarization curves and electrochemical impedance spectroscopy (EIS), in a three-electrode cell setup with steel as the working electrode. Prior to the experiments, the working electrode was subjected to 30 minutes of free corrosion to establish a quasi-stationary corrosion potential (Ecorr). Subsequently, polarization curves and EIS measurements were generated using a PGZ100 potentiostat and analyzed with EC-Lab V 9.97 software.

### 2.4. SEM/EDX

Surface morphological investigations were conducted using SEM and EDX to validate the electrochemical findings. Steel samples, both with and without Q-Cl and Q-H, were submerged in a 1 M HCl solution for 6 h and analyzed using the Quanta FEG 450 to produce SEM images. EDX analysis was performed in tandem with SEM investigations.

### 2.5. ICP spectrometry

The elemental composition and ion concentration of mild steel surfaces were examined using inductively coupled plasma (ICP) spectrometry. This evaluation was conducted under two conditions: without any added corrosion-inhibiting molecules and with them. Specifically, the mild steel substrate was immersed in two different solutions: 1.0 M hydrochloric acid and 1.0 M hydrochloric acid containing Q-Cl and Q-H inhibitors, for a period of 6 hours at a temperature of 298 K. The results of our investigation indicate that the addition of Q-Cl and Q-H inhibitors to the HCl solution reduces the concentration of ions generated on the mild steel surface, demonstrating the successful inhibition of corrosion by these inhibitors. These findings have practical implications for the development of new corrosion inhibitors specifically designed for mild steel in aggressive environments.

**Table 1**
Mass content of impurities present in the studied plain steel.

| Elements | C | Si | Mn | Cr | Mo | Ni | Al | Co | Cu | V | W | Fe |
|---|---|---|---|---|---|---|---|---|---|---|---|---|
| Teneur % | 0.11 | 0.24 | 0.47 | 0.12 | 0.02 | 0.1 | 0.03 | <0.0012 | 0.14 | <0.003 | 0.06 | 98.7 |

### 2.6. Theoretical details

The inhibitory properties of the studied organic molecules and their chemical reactivity were evaluated using density functional theory (DFT). Theoretical calculations were performed using Gaussian 09 software [19] with the B3LYP hybrid functional and the 6-311G(d,p) basis set [20]. The electronic properties, such as the energies of the highest occupied molecular orbital (EHOMO) and the lowest occupied molecular orbital (ELUMO), as well as their energy gap (ΔEgap), hardness (η), softness (σ), global electrophilicity, global nucleophilicity (ε), back donation energy (ΔEb-d), and fraction of transferred electrons (ΔN), were determined and analyzed. Moreover, Fukui indices were used to evaluate the chemical reactivity of the studied inhibitor molecules. The DFT calculations for the inhibitor molecules were performed in an aqueous medium using water as the solvent. The integral equation formalism of the polarizable continuum model (IEFPCM) was employed to account for solvent effects in the calculations [21].

## 3. Result and discussion

### 3.1. Electrochemical studies

#### 3.1.1. OCP

Prior to conducting electrochemical experiments, mild steel electrodes were immersed in the solution for 1800s, and open circuit potentials (OCPs) were recorded. Fig. 1 illustrates the OCP profiles for mild steel samples in a 1.0 M HCl solution, both with and without varying concentrations of Q-Cl and Q-H inhibitors, at 298 K. The plots reveal that the corrosion inhibitors significantly influence the OCP compared to the blank solution. The observed shifts in OCP are due to the adsorption of the inhibitors onto the metal electrode surface, which displaces corrosive species from the solution and alters the surface state of the electrode. These findings provide evidence of the inhibitors' adsorption on the metal surface.

#### 3.1.2. EFM

Electrochemical Frequency Modulation (EFM) is a non-destructive method for measuring corrosion, providing an estimate of the corrosion current. EFM involves subjecting the cell to two sine waves simultaneously, each at a different frequency. The system's response to potential stimulation is non-linear due to the non-linear relationship between current and potential. Furthermore, the current response includes not only the two input frequencies but also various frequency components, such as multiples, differences, and the cumulative total of the input frequencies. These frequencies are deliberately selected rather than chosen randomly. Opting for both frequencies as extremely small integer multiples of the base frequency determines the experiment's duration. Representative waveforms for the frequency spectrum of mild steel in 1.0 M HCl medium are illustrated in Fig. 2, showing input frequencies of 2 Hz and 5 Hz, both in the presence and absence of variable concentrations of Q-H and Q-Cl.

To ensure accurate measurements, the higher frequency used in Electrochemical Frequency Modulation (EFM) experiments should be at least twice the lower frequency. This frequency ratio helps achieve reliable results by mitigating the influence of double layer charging on the current response [22]. Typically, the upper frequency limit is set around 10 Hz to maintain a moderate frequency range. The intermodulation spectra obtained from EFM experiments are shown in Fig. 3, where each spectrum plots the current response as a function of frequency. The corrosion kinetic parameters detailed in Table 3 were determined using the EFM technique, applying the relevant equations to analyze the data and derive the parameters.

$$i_{corr} = \frac{i_\omega^2}{\sqrt{48(2i_\omega i_{3\omega} - i_{2\omega})}} \tag{1}$$

$$\beta_a = \frac{i_\omega U_0}{2i_{2\omega} + 2\sqrt{3}\sqrt{2i_\omega i_\omega - i_{2\omega}^2}} \tag{2}$$

$$\beta_a = \frac{i_\omega U_0}{2\sqrt{3}\sqrt{2i_{3\omega}i_\omega - i_{2\omega}^2 - 2i_{2\omega}}} \tag{3}$$

The notation "$i_\omega$" indicates the instantaneous current density recorded for the working electrode at frequency "$\omega$," while "$U_0$" stands for the amplitude of the sine wave distortion.

In addition to measuring corrosion rate and Tafel parameters, EFM also captures causality factors 2 and 3. These additional variables serve to corroborate the acquired data.

$$Casuality\ factor(2) = \frac{i_{\omega_2} \pm \omega_1}{i_{2\omega_1}} = 2.0 \tag{4}$$

$$Casuality\ factor(3) = \frac{i_{2\omega_2} \pm \omega_1}{i_{3\omega_1}} = 3.0 \tag{5}$$

Inhibition efficiency values ($E_{EFM}$ (%)) presented in Table 3 were calculated from Eq. (5) [23]:
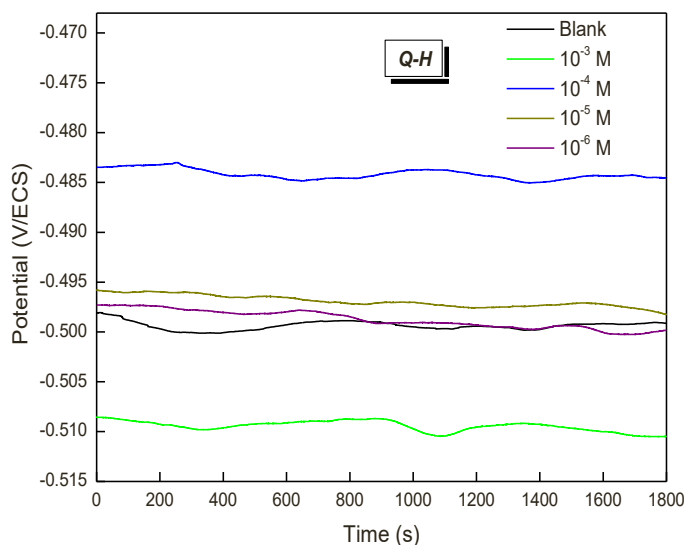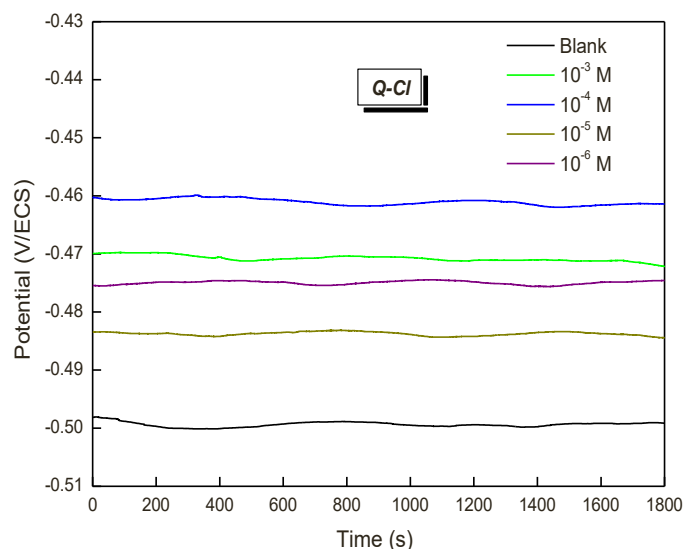


**Fig. 1.** Open circuit potential with time in HCl medium at 298 K.
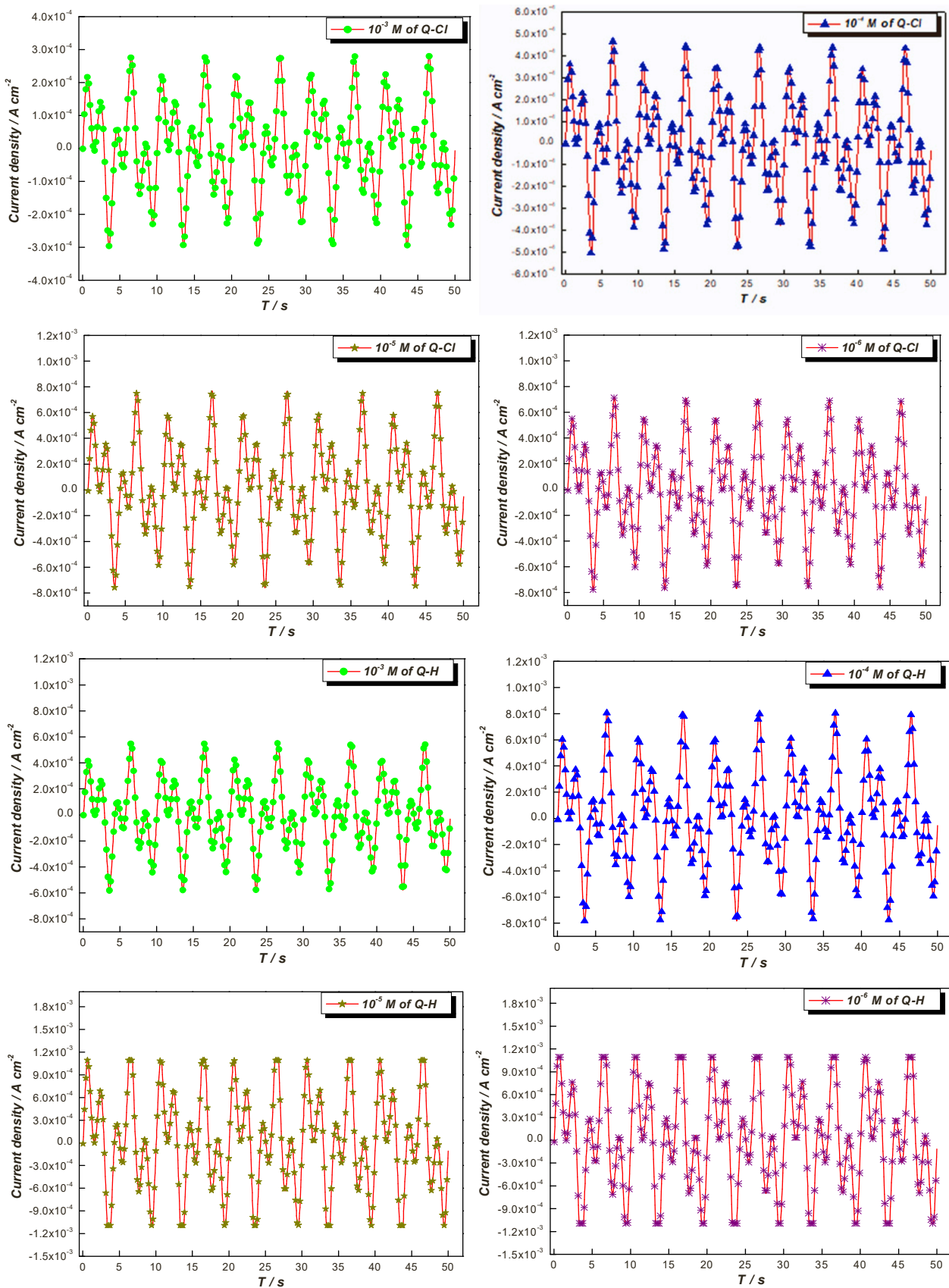
**Fig. 2.** Waveform spectrum depicting input frequencies of 2 Hz and 5 Hz for mild steel in 1.0 M HCl, with and without varying concentrations of Q-H and Q-Cl.

$$E_{EFM} \quad \% = \quad 1 \frac{-i_{corr}}{i_{corr}^0} \times 100 \tag{6}$$

where $i_{corr}^0$ represents the corrosion current density without the inhibitor, and $i_{corr}$ denotes the corrosion current density in the presence of the inhibitor.

When mild steel is exposed to a 1 M HCl solution without any inhibitors, the corrosion current density ($i_{corr}$) is higher, indicating more severe corrosion. However, as shown in Table 3, when inhibitors are added, the corrosion current density decreases, and the inhibition efficiency (EEFM %) increases as the concentration of the inhibitors rises. This suggests that the inhibitors are likely forming a protective layer by adsorbing onto the metal surface, reducing corrosion [24]. Among the inhibitors tested, Q-H shows higher inhibition efficiency than Q-Cl. Furthermore, the causality factors, CF-2 and CF-3, which correspond to theoretical values of 2 and 3 respectively, are derived from the frequency spectrum of the current response. The close match between these experimentally obtained causality factors and the theoretical values confirms the reliability of the data.



**Fig. 3.** Intermodulation spectrum for Mild steel in 1.0 M HCl in absence and presence of various concentrations of Q-H and Q-Cl.

**Fig. 3.** (*continued*).

**Table 3**
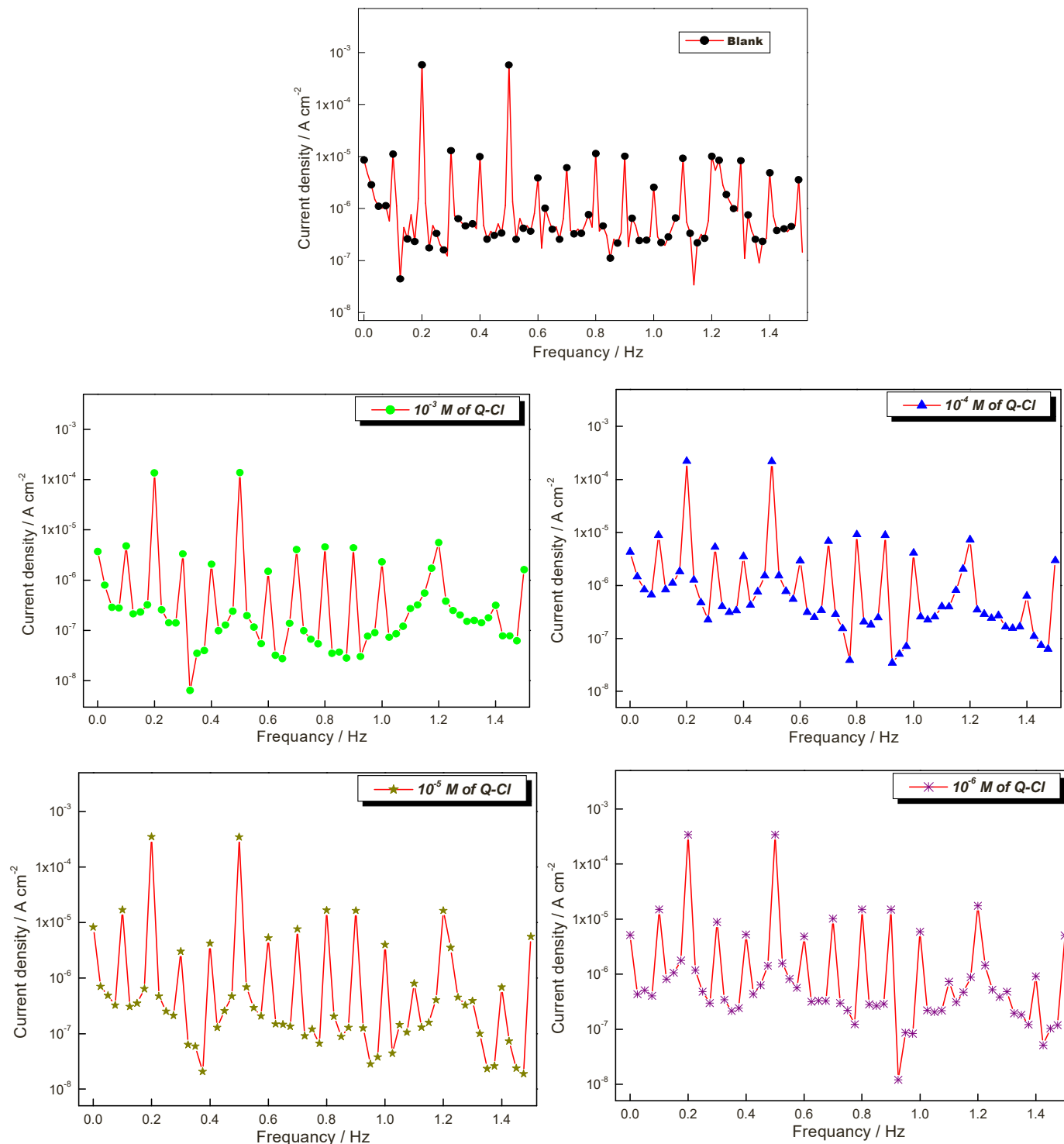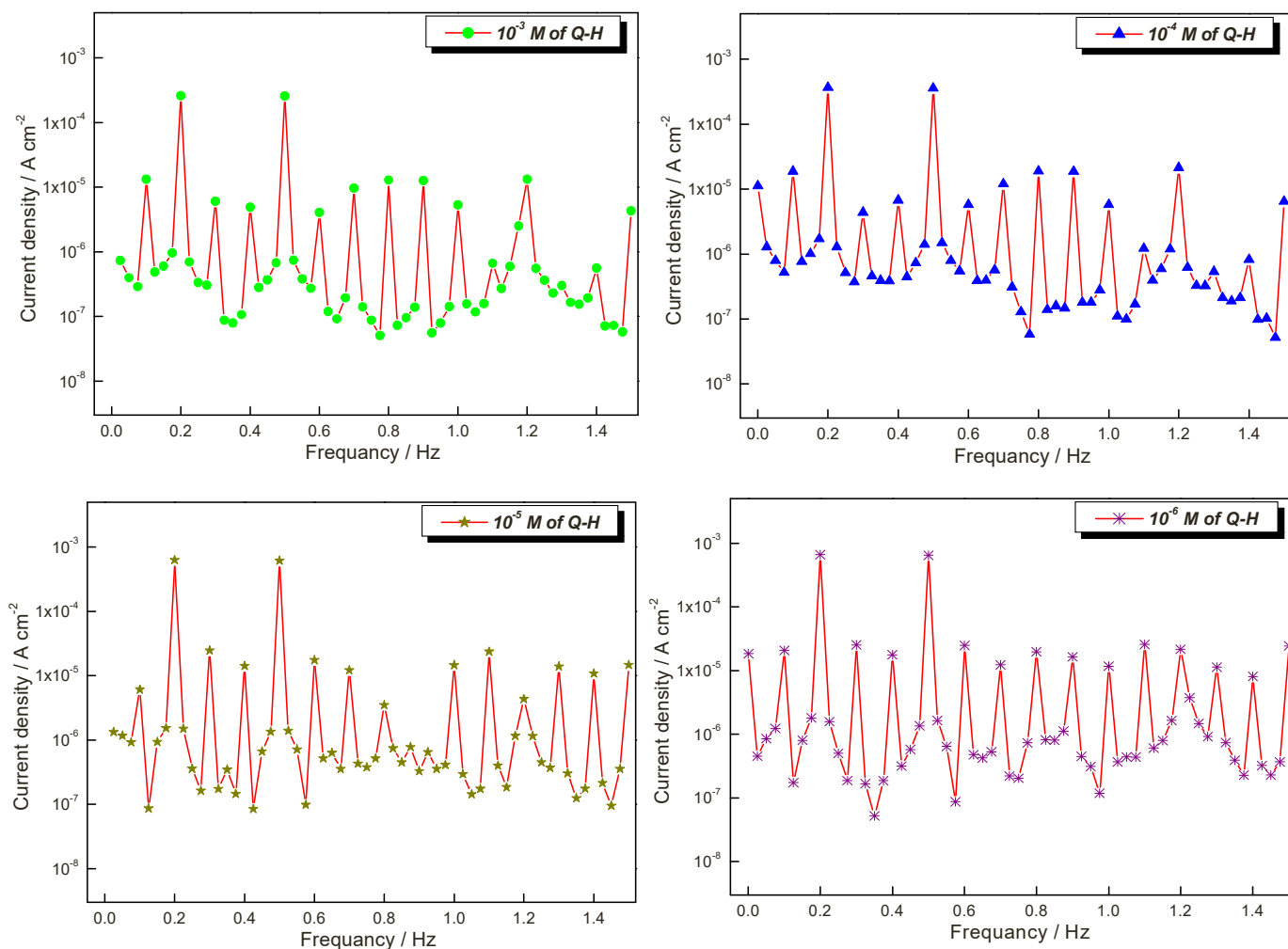Electrochemical kinetic parameters obtained by EFM technique for Mild steel in absence and presence of Q-H and Q-Cl in 1.0 M HCl at 298 K.

| | Conc. M | $i_{corr}$ µA cm$^{-2}$ | $\beta_c$ mV dec$^{-1}$ | $\beta_a$ mV dec$^{-1}$ | CR mpy | $E_{EFM}$ % | C.F-2 | C.F-3 |
|---|---|---|---|---|---|---|---|---|
| **1.0 M HCl** | – | **755** | **162** | **177** | **344.9** | – | **1.52** | **2.86** |
| **Q-Cl** | $10^{-6}$ | 138.5 | 103 | 113 | 75.4 | 81.6 | 1.70 | 3.15 |
| | $10^{-5}$ | 122.6 | 103 | 108 | 62.5 | 83.7 | 1.30 | 3.05 |
| | $10^{-4}$ | 96.8 | 111 | 123 | 49.9 | 87.1 | 1.59 | 2.91 |
| | $10^{-3}$ | 68.3 | 116 | 129 | 35.8 | 90.9 | 1.68 | 3.11 |
| **Q-H** | $10^{-6}$ | 231.9 | 126 | 142 | 134.3 | 69.3 | 1.27 | 2.79 |
| | $10^{-5}$ | 217.2 | 105 | 112 | 116.4 | 71.2 | 1.28 | 2.22 |
| | $10^{-4}$ | 166.1 | 96 | 103 | 86.2 | 78.0 | 1.30 | 3.18 |
| | $10^{-3}$ | 125.6 | 98 | 108 | 63.9 | 83.3 | 1.53 | 3.11 |

### 3.1.3. Polarization studies

The kinetics of mild steel corrosion in acidic conditions were assessed using potentiodynamic polarization experiments, as shown in Fig. 4. The results revealed that the presence of Q-Cl and Q-H inhibitors in the 1.0 M HCl solution influenced both the anodic and cathodic processes [25]. This behavior is attributed to the adsorption of inhibitors, which effectively restricts metal solubility and delays the reduction of hydrogen ions. Notably, all cathodic segments maintain their parallel configuration, indicating that the Q-Cl and Q-H inhibitors have minimal impact on the hydrogen ion reduction process. Therefore, the main mechanism for hydrogen release remains a charge transfer process [26,27].

Table 4 presents the electrochemical characteristics for various concentrations of Q-Cl and Q-H inhibitors in 1 M HCl. These include the

anodic Tafel slopes ($\beta a$), cathodic Tafel slopes ($\beta c$), corrosion potential ($E_{corr}$), corrosion current density ($i_{corr}$), and inhibition efficiency ($\eta pp$ %). The inhibition efficiency ($\eta pp$%) was calculated using the following equation [28]:

$$\eta pp\% = \frac{i_{corr}^0 - i_{corr}}{i_{corr}^0} \times 100 \tag{7}$$

The corrosion current density of the blank solution is denoted by $i_{corr}^0$, while that of the inhibited solution is denoted by $i_{corr}$.

The results presented in Table 4 illustrate the impact of varying concentrations of Q-Cl and Q-H inhibitors on the electrochemical parameters of mild steel exposed to a 1 M HCl solution. As the
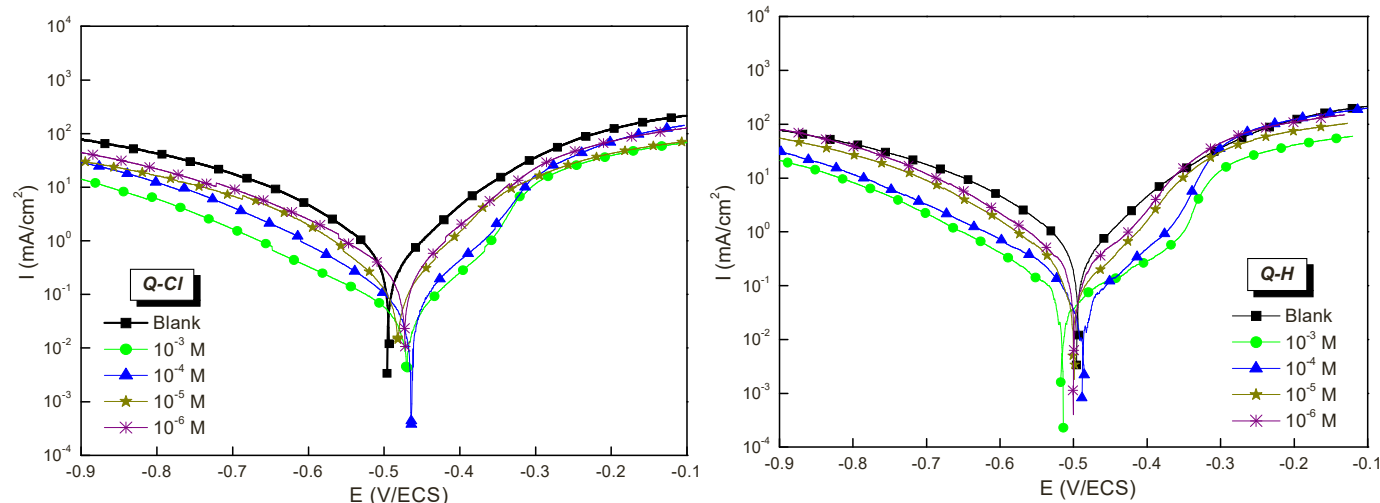
**Fig. 4.** Tafel polarization curves for mild steel in 1.0 M HCl with and without of different concentrations of Q-Cl and Q-H.

**Table 4**

Polarization parameters for mild steel in 1.0 M HCl without and with of various concentrations of Q-Cl and Q-H.

| Medium | Conc. M | $-E_{corr}$ mV/ ECS | $i_{corr}$ μA cm$^{-2}$ | $-\beta_c$ mV dec$^{-1}$ | $\beta a$ mV dec$^{-1}$ | $\eta_{PP}$ % |
|---|---|---|---|---|---|---|
| **1 M HCl** | – | $498 \pm 5$ | $983 \pm 6$ | $140 \pm 4$ | $150 \pm 5$ | - |
| **Q-Cl** | $10^{-6}$ | $473 \pm 4$ | $167 \pm 3$ | $136 \pm 5$ | $140 \pm 4$ | 83.0 |
| | $10^{-5}$ | $483 \pm 6$ | $153 \pm 5$ | $132 \pm 4$ | $135 \pm 6$ | 84.4 |
| | $10^{-4}$ | $460 \pm 5$ | $105 \pm 4$ | $126 \pm 3$ | $130 \pm 5$ | 89.3 |
| | $10^{-3}$ | $471 \pm 3$ | $83 \pm 2$ | $128 \pm 5$ | $129 \pm 4$ | 91.5 |
| **Q-H** | $10^{-6}$ | $498 \pm 5$ | $284 \pm 4$ | $138 \pm 3$ | $145 \pm 5$ | 71.1 |
| | $10^{-5}$ | $497 \pm 4$ | $252 \pm 5$ | $134 \pm 4$ | $142 \pm 4$ | 74.3 |
| | $10^{-4}$ | $483 \pm 6$ | $195 \pm 4$ | $132 \pm 5$ | $139 \pm 3$ | 80.2 |
| | $10^{-3}$ | $509 \pm 5$ | $145 \pm 3$ | $129 \pm 2$ | $136 \pm 4$ | 85.2 |

concentration of these inhibitors increases, there is a notable reduction in corrosion current density ($i_{corr}$) and a corresponding increase in inhibition efficiency. Specifically, at the optimal concentration of $10^{-3}$ M, the corrosion current density decreases to 83 μA cm$^2$ for Q-Cl and to 145 μA cm$^2$ for Q-H. This reduction indicates that both inhibitors are effective in decreasing the rate of corrosion. Additionally, the percentage inhibition efficiency (ηpp%) rises with the concentration of the inhibitors, reaching 91.5 % for Q-Cl and 85.2 % for Q-H. These values show that both Q-Cl and Q-H significantly improve corrosion resistance, with Q-Cl being slightly more effective [29].

In contrast, the corrosion potential ($E_{corr}$) values exhibit only slight variations, not exceeding 27 mV/SCE. This stability in $E_{corr}$ suggests that the inhibitors primarily function as mixed-type inhibitors and act as adsorbent inhibitors. Rather than significantly altering the fundamental reaction mechanism of corrosion, the inhibitors provide protection by forming a layer on the metal surface [30]. Therefore, the minimal change in $E_{corr}$ supports the idea that the inhibitors work through adsorption rather than changing the corrosion process itself. Overall, the use of both Q-Cl and Q-H inhibitors in a 1 M HCl solution proves beneficial, with Q-Cl showing slightly superior inhibition efficiency, while the consistent $E_{corr}$ values confirm the adsorption-based mechanism of inhibition.

### 3.1.4. EIS studies

The EIS spectra were analyzed using a Randle electrical equivalent circuit model, which includes important parameters such as the charge transfer resistance (Rct), solution resistance (Rs), and constant phase element (CPE). The NYQUIST plots are presented in Fig. 5, while the BODE plots can be found in Fig. 6. The electrical equivalent circuit used

in the analysis is depicted in Fig. 7, and the resulting data are summarized in Table 5. The corrosion inhibition efficiency and other parameters were calculated using the following equations:

$$\eta_{imp}\% = [(R_{ct} - R_{ct}^0) / R_{ct} *100]; \; \theta = (R_{ct} - R_{ct}^0) / R_{ct} \qquad (8)$$

Fig. 5 illustrates the Nyquist plots obtained with and without the presence of our inhibitors. These plots reveal the appearance of a single capacitive loop, indicating that the charge transfer mechanism predominantly controls the corrosion response. Additionally, an increase in the resistance of the inhibitor film layer to charge transfer is correlates with the diameter of the semicircle. The formation of a protective coating on the mild steel surface by both inhibitors (Q-Cl and Q-H) may explain these results [31,32]. The semicircular loops display a depression, which may be attributed to both the geometric nature of the current distribution and the heterogeneity and roughness of the mild steel surface [33]. The variation of the Nyquist plot with respect to the semicircle diameter is comparable to the variation observed in the Bode plot with different concentrations of Q-Cl and Q-H. All phase-frequency angle curves exhibit a single wave, supporting the single constant indicated in the Nyquist plot.

Furthermore, Table 5 provides evidence that the charge transfer resistance (Rct) increases as the concentration of both Q-Cl and Q-H inhibitors is increases in the aggressive HCl medium. This increase in Rct is attributed to the formation of a protective layer at the metal/solution interface, which impedes the corrosion process [34]. At the optimal concentration of $10^{-3}$ M, both Q-Cl and Q-H exhibit substantial inhibitory effectiveness. Specifically, Q-Cl achieves an inhibition efficiency of 91.6 %, while Q-H achieves 84.9 %. These efficiency values reflect the extent to which each inhibitor reduces the corrosion rate. The observed strong correlation between the inhibition efficiencies obtained from different analytical techniques—namely, corrosion rate measurements, Electrochemical Impedance Spectroscopy (EIS), and Potentiodynamic Polarization (PDP)—supports the conclusion that Q-Cl is more effective than Q-H. This correlation highlights the reliability and consistency of the inhibition performance of Q-Cl across various methods of evaluation.

### 3.2. Adsorption isotherm

To gain a deeper insight into the adsorption behavior of Q-Cl and Q-H inhibitors on mild steel surfaces, we employed various adsorption isotherm models, including Langmuir, Freundlich, Temkin, and Frumkin. These models were used to analyze the adsorption process and understand the interaction between the inhibitors and the metal surface.
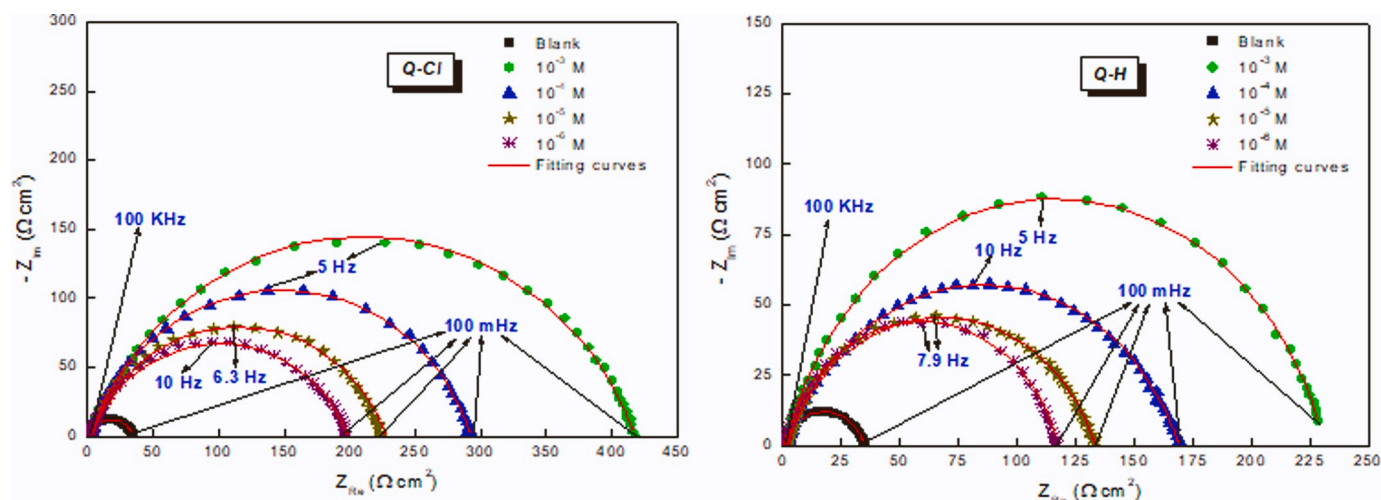
**Fig. 5.** NYQUIST plots of mild steel in 1.0 M HCl solution with and without different concentrations of Q-Cl and Q-H.
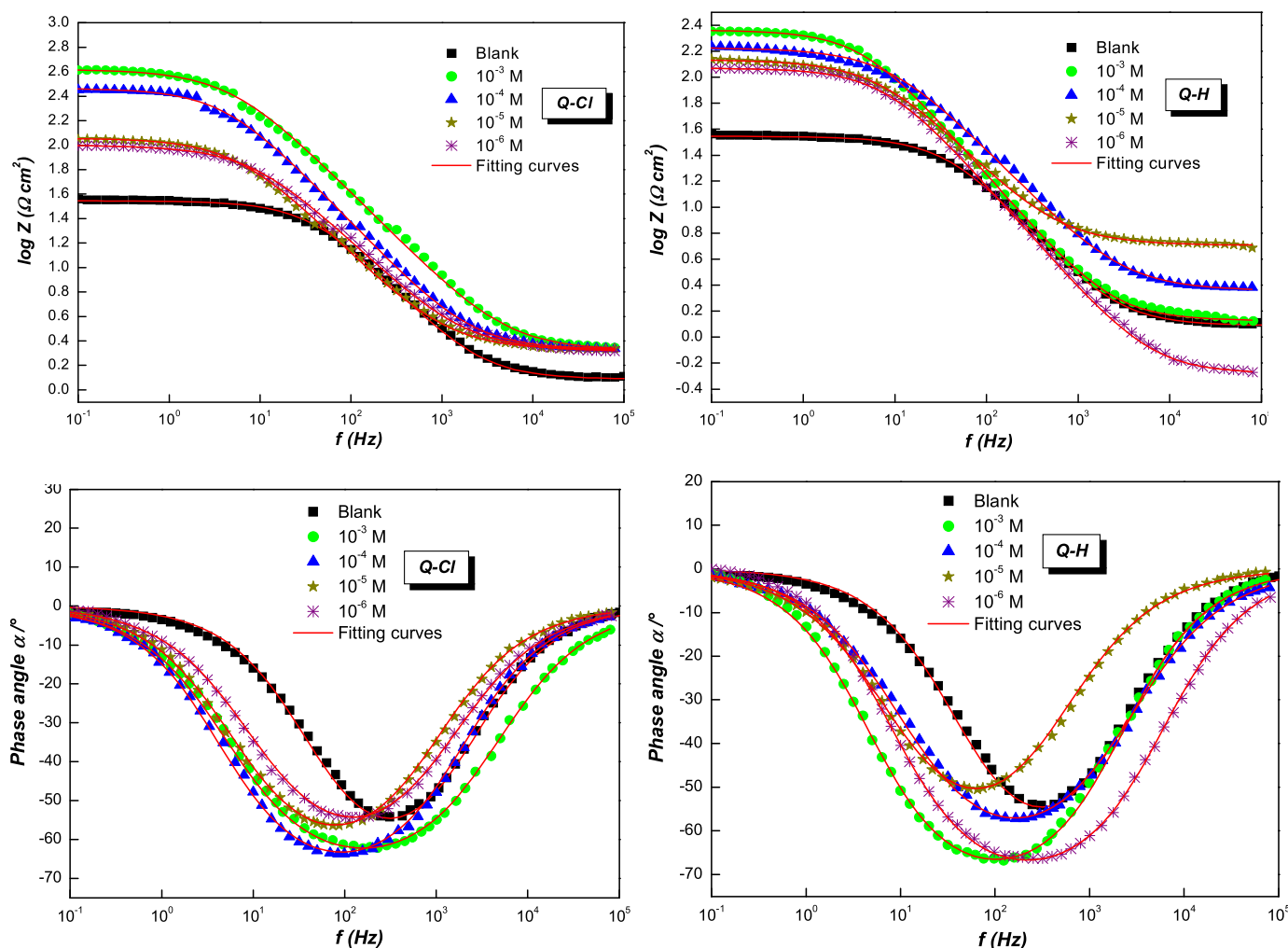


**Fig. 6.** Bode's plots and Phase angle for mild steel in 1.0 M HCl solution with and without different concentrations of Q-Cl and Q-H.

The data for these analyses were obtained from Electrochemical Impedance Spectroscopy (EIS) measurements. Table 6 presents the linear equations corresponding to each of the adsorption isotherm models, which are used to fit the experimental data. Fig. 8 illustrates the fitted data, showing how well each model describes the adsorption behavior of the inhibitors. By comparing the results from these different models, we aimed to determine the most appropriate model that accurately represents the adsorption mechanism of Q-Cl and Q-H on mild steel

Fig. 8 depicts the linear fitting obtained through the electrochemical approach for both inhibitors, and the corresponding adsorption
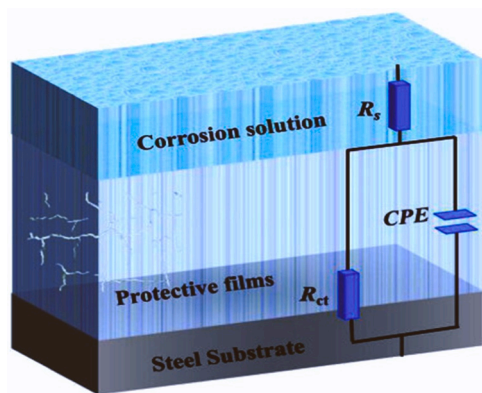
**Fig. 7.** Electrochemical equivalent circuit used to fit the impedance and BODE's spectra.

parameters derived from various isotherms are presented in Table 7. Among the tested isotherm models, it is evident that Q-Cl and Q-H exhibit conform with the Langmuir isotherm, as evidenced by the high regression coefficient ($R^2 = 1$) and a substantial deviation of the slope from unity for both inhibitors. This suggests that the Langmuir model is suitable for describing the adsorption process, which is supported by previous research [35]. According to this model, the metal surface possesses a fixed number of adsorption sites, with each site accommodating a single adsorbed inhibitor molecule.

In contrast, the adsorption constants (Kads) derived from the Freundlich isotherm are relatively low, suggesting that this model does not fit the adsorption data as well as others. Moreover, the regression coefficients for the Frumkin and Temkin isotherms are also low, despite the relatively higher Kads values obtained from these models. This indicates that the adsorption behavior of the inhibitors does not align well with the assumptions of the Frumkin and Temkin isotherms. To further evaluate the adsorption characteristics, the standard free energy of adsorption ($\Delta G_{ads}$) can be determined using the Van't Hoff Eq. (10) [36, 37]. This calculation will provide additional insight into the thermodynamic aspects of the adsorption process.

$$\Delta G_{ads} = -RT\ln(55.5K_{ads}) \tag{9}$$

where the molar concentration of water in the solution is 55.5, the thermodynamic temperature (in this case, 298 K), and R represents the universal gas constant.

According to the data presented in Table 7, the standard free energy of adsorption ($\Delta G_{ads}$) for Q-Cl and Q-H is approximately −42.8 kJ/mol and −41.1 kJ/mol, respectively. These negative values suggest that the adsorption of Quinazoline molecules onto the steel surface involves a chemical adsorption process, which is typically characterized by stronger interactions between the inhibitor molecules and the metal surface [38]. The magnitude of these $\Delta G_{ads}$ values indicates that the adsorption

is spontaneous and likely involves the formation of chemical bonds. Furthermore, the adsorption–desorption equilibrium constants (Kads) for both Q-Cl and Q-H, also provided in Table 7, are notably high. This reflects a strong affinity of these inhibitors for the steel surface, implying that once the Quinazoline molecules adsorb onto the surface, they tend to remain attached, effectively protecting the steel from corrosion [39]. The high Kads values further reinforce the conclusion that these inhibitors exhibit strong and stable adsorption behavior, making them effective at mitigating corrosion in harsh environments.

### 3.3. Thermodynamic parameters and temperature effects

Temperature is a critical parameter that can impact corrosion effectiveness in an aggressive solution. It can accelerate mild steel's reaction with an aggressive solution, whether inhibitors are present or not. The present investigation evaluated the polarization curves of MS in 1.0 M HCl, both with and without $10^{-3}$ M of our inhibitors Q-Cl and Q-H, at various temperatures ranging from 298 K to 328 K. The findings are displayed in Fig. 9, and Table 8 provides a summary of the associated electrochemical parameters. The polarization curves with and without

**Table 6**
Different isotherms linear equations.

| isotherm | *Forme linéaire* | *Courbe* |
|---|---|---|
| Langmuir | $k_{ads}c_{inh} = \dfrac{\theta}{1-\theta}$ | $\dfrac{C_{inh}}{\theta} vs C_{inh}$ |
| Temkin | $e^{-2f\theta} = k_{ads}C_{inh}$ | $\theta vs \ln(C\|inh)$ |
| Freundluich | $\theta = k_{ads}C_{inh}^n$ | $\ln(\theta) vs \ln(C_{inh})$ |
| Frumkin | $\dfrac{\theta}{1-\theta}e^{-2f\theta} = k_{ads}C_{inh}$ | $\ln\left(C_{inh}\dfrac{1-\theta}{\theta}\right) vs \theta$ |



**Fig. 8.** Different adsorption isotherms of mild steel in 1.0 M HCl in the presence of Q-Cl and Q-H.

**Table 5**
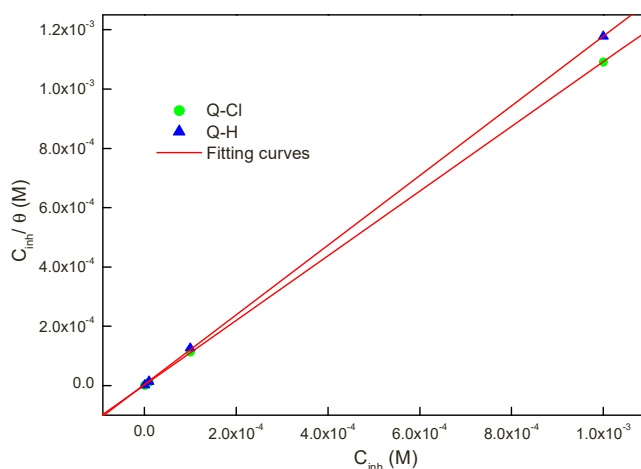Impedance parameters for mild steel in 1.0 M HCl solution in absence and addition of different concentrations of Q-Cl and Q-H.

| | Conc. (M) | $R_s$ ($\Omega$ cm$^2$) | $R_{ct}$ ($\Omega$ cm$^2$) | $C_{dl}$ ($\mu$F.cm$^{-2}$) | $n_{dl}$ | Q ($\Omega^{-1}$ S$^n$ cm$^{-2}$) | $\Theta$ | $\eta_{imp}$ % |
|---|---|---|---|---|---|---|---|---|
| 1 M HCl | – | 1.12 ± 0.3 | 34.7 ± 0.6 | 121.0 | 0.773 ± 0.02 | 419 ± 2.8 | - | - |
| Q-Cl | $10^{-6}$ | 2.0 ± 0.1 | 197 ± 0.4 | 96.8 | 0.736 ± 0.01 | 345.7 ± 2.0 | 0.824 | 82.4 |
| | $10^{-5}$ | 2.1 ± 0.2 | 225 ± 0.4 | 88.7 | 0.780 ± 0.008 | 284.6 ± 1.8 | 0.845 | 84.5 |
| | $10^{-4}$ | 2.1 ± 0.3 | 291 ± 0.3 | 84.6 | 0.803 ± 0.004 | 243.0 ± 1.7 | 0.881 | 88.1 |
| | $10^{-3}$ | 2.0 ± 0.2 | 416 ± 0.4 | 75.0 | 0.773 ± 0.002 | 164.6 ± 1.4 | 0.916 | 91.6 |
| Q-H | $10^{-6}$ | 1.0 ± 0.1 | 117 ± 0.4 | 112.6 | 0.820 ± 0.008 | 338.4 ± 2.4 | 0.703 | 70.3 |
| | $10^{-5}$ | 1.5 ± 0.2 | 132 ± 0.5 | 102.8 | 0.772 ± 0.009 | 318.9 ± 2.3 | 0.737 | 73.7 |
| | $10^{-4}$ | 2.2 ± 0.3 | 167 ± 0.3 | 97.4 | 0.765 ± 0.005 | 256.0 ± 1.6 | 0.792 | 79.2 |
| | $10^{-3}$ | 1.3 ± 0.2 | 230 ± 0.4 | 86.5 | 0.830 ± 0.01 | 266.8 ± 1.5 | 0.849 | 84.9 |

**Table 7**

Adsorption parameters deducted from linearizing various adsorption isotherms for mild steel corrosion in 1.0 M HCl in the presence of Q-Cl and Q-H at 298 K.

| Isothermes | Parameters | *Q-Cl* | *Q-H* |
|---|---|---|---|
| *Langmuir* | $R^2$ | 0.99999 | 0.99998 |
| | $K_{ads}$ *(L mol⁻¹)* | 568.2 10³ | 290.6 10³ |
| | *Slope* | 1.0 | 1.1 |
| | $\Delta G_{ads}$ *(KJ/mol)* | −42.8 | −41.1 |

Q-Cl and Q-H are all parallel to one another, as shown in Fig. 9, suggesting that temperature has no effect on the protective mechanism [40]. Furthermore, an increase in temperature encourages the desorption of adsorbed molecules, which accounts for the corresponding rise in current density.

The findings in Table 8 show that as the temperature of the solution rises, the corrosion current densities of mild steel also increase. However, this effect is more pronounced when inhibitors are not present compared to when Q-Cl and Q-H compounds are used. Moreover, it is observed that the temperature somewhat reduces the inhibition efficiency (ηpp%), which might be due to the desorption of inhibitor molecules from the steel substrate [41]. The maximum ηpp% values were 83.6 % for Q-Cl and 77.6 % for Q-H, demonstrating the effectiveness of these two inhibitors in **mitigating** steel corrosion in 1.0 M hydrochloric acid solution.

The thermodynamic condition of the metal/Corrosive solution system are analyzed using the data presented in Table 8. This analysis includes examining the activation parameters for the system both in the presence and absence of Q-Cl and Q-H inhibitors. These parameters provide information about how the metal surface responds to changes in the physical and chemical factors of the solution. The primary parameter, $E_a$, which represents the activation energy required for the reaction to proceed. Ea is crucial for understanding the reaction rate: a higher activation energy indicates a slower reaction, while a lower activation energy suggests a faster reaction. By evaluating the activation energy, we can assess how the presence of inhibitors affects the rate of corrosion. The activation energy of the corrosion process can be determined using the Arrhenius Eq. (11) [42], which allows for the calculation of Ea based on temperature and reaction rate data. This equation provides a quantitative measure of how the corrosion rate changes with temperature, offering further insight into the effectiveness of the inhibitors in altering the corrosion dynamics of the metal surface.

$$i_{corr} = Ae^{\frac{-Ea}{RT}} \tag{10}$$

Where $i_{corr}$ is the corrosion current density, A is the pre-exponential factor, $E_a$ is the apparent activation energy, R is the gas constant (R= 8.314 J.mol⁻¹. K⁻¹) and T is the absolute temperature.

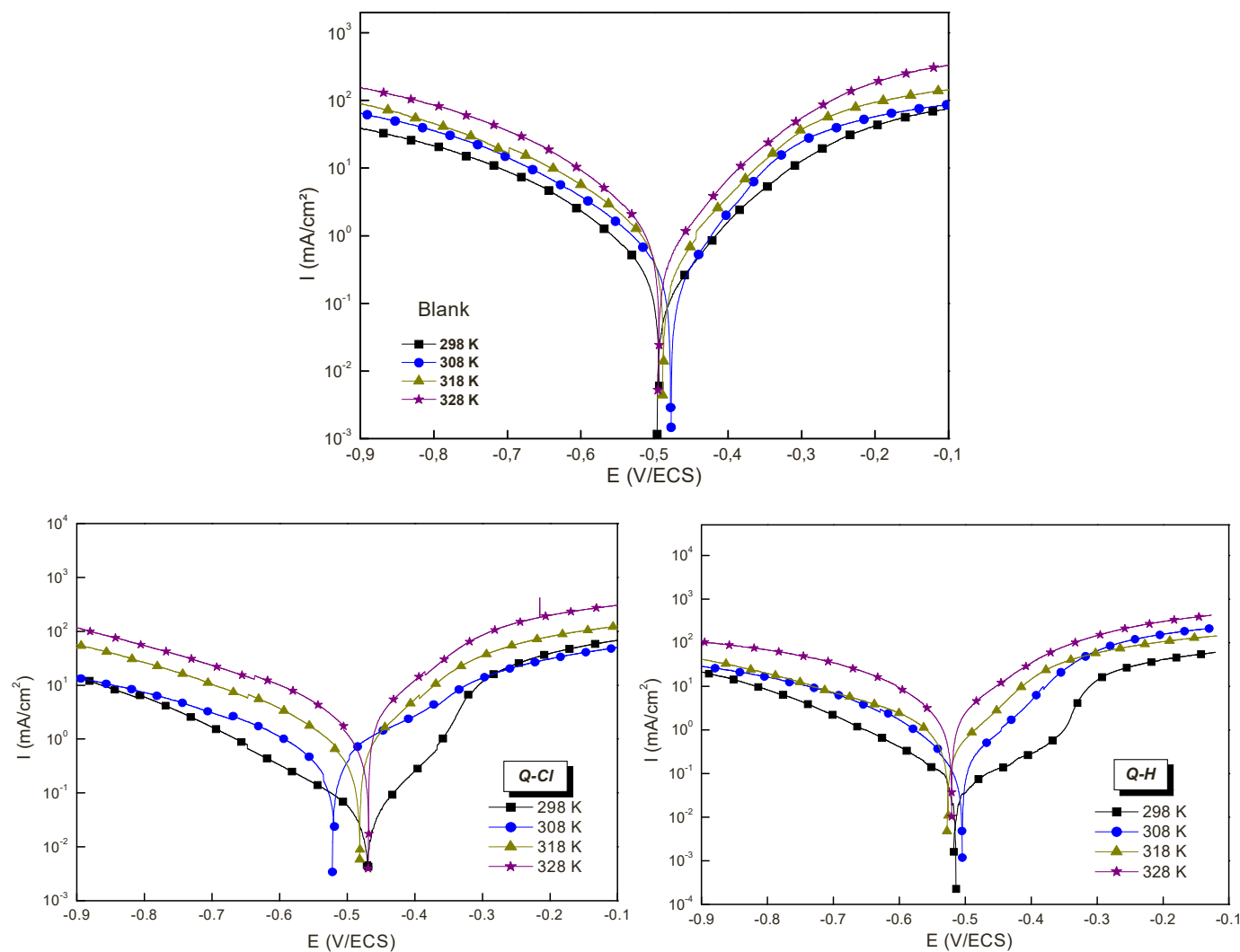To gain a better understanding of the corrosion reaction processes, it



**Fig. 9.** Effect of temperature on the polarization curves of mild steel in 1 M hydrochloric acid solution without and with $10^{-3}$ M of Q-Cl and Q-H at different temperatures from 298 to 328 K.

**Table 8**

Temperature effects on mild steel electrochemical parameters and Activation parameters Ea, ΔHa and ΔSa in 1 M hydrochloric acid present and absent $10^{-3}$ M of Q-Cl and Q-H addition.

| Compounds | Tempe K | $-E_{corr}$ mV/ECS | $i_{corr}$ µA cm$^{-2}$ | $-\beta_c$ mV dec$^{-1}$ | $\beta a$ mV dec$^{-1}$ | $\eta_{PP}$ % | Ea (KJ/mol) | ΔHa (KJ/mol) | ΔSa (J/mol K) |
|---|---|---|---|---|---|---|---|---|---|
| Blank | 298 | 498 | 983 | 140 | 150 | - | 21.0 | 18.5 | −126.0 |
|  | 308 | 477 | 1200 | 184 | 112 | - |  |  |  |
|  | 318 | 487 | 1450 | 171 | 124 | - |  |  |  |
|  | 328 | 493 | 2200 | 161 | 118 | - |  |  |  |
| Q-Cl | 298 | 471 | 83 | 128 | 129 | 91.5 | 38.8 | 36.2 | −86.8 |
|  | 308 | 515 | 128 | 172 | 109 | 89.3 |  |  |  |
|  | 318 | 477 | 192 | 163 | 119 | 86.7 |  |  |  |
|  | 328 | 464 | 359 | 154 | 115 | 83.6 |  |  |  |
| Q-H | 298 | 509 | 145 | 129 | 136 | 85.2 | 32.4 | 29.8 | −104.0 |
|  | 308 | 500 | 198 | 145 | 110 | 83.5 |  |  |  |
|  | 318 | 522 | 278 | 162 | 122 | 80.8 |  |  |  |
|  | 328 | 518 | 492 | 156 | 113 | 77.6 |  |  |  |

is essential to consider two energy components: the enthalpy of activation (ΔHa) and the entropy of activation (ΔSa). These energies govern the differences in heat and disorder, respectively. The application of these equations is demonstrated in Fig. 10, and the corresponding results are summarized in Table 8.

$$\ln\left(\frac{i_{corr}}{T}\right) = \left[\ln\left(\frac{R}{hN_a}\right) + \left(\frac{\Delta S_a}{R}\right)\right] - \frac{\Delta H_a}{RT} \qquad (11)$$

Where Avogadro's number (Na), apparent activation energy (Ea), and Planck's constant (h)

In our study, we observed that the activation energy value obtained in the absence of Q-Cl and Q-H inhibitors was lower than when they were present. This indicates that the presence of Q-Cl and Q-H in the solution reduces the corrosion current density, likely due to the adsorption process. Furthermore, we found that the oxidation of Fe to $Fe^{2+}$ at the electrode-electrolyte interface was diminished in the presence of Q-Cl and Q-H, suggesting that the charge transfer at the contact is influenced by these inhibitors. This phenomenon is likely caused by a reduction in the surface area available for metal oxidation, leading to increased effectiveness in corrosion inhibition.

Additionally, the positive values of activation enthalpy (ΔHa) indicate that the corrosion of mild steel is an endothermic process, requiring additional energy for the oxidation reaction to occur [43]. This endothermic nature suggests that corrosion becomes more challenging in the presence of these inhibitors. The negative values of entropies (ΔSa) suggest a behavior characterized by reduced disorderliness. This is likely attributed to the rate-determining phase involving an activated complex, indicating an association phase rather than a dissociation stage. In

a dissociation stage, disorder would diminish as reactants transition from reactants to the activated complex [44].

### 3.4. Surface analysis

#### a. SEM/EDX

To further our understanding of the adsorption process behind corrosion prevention, we examined the surface morphologies and EDX spectra of the mild steel substrate. The results of this study are presented in Table 9 and Fig. 11. The surface morphology of the mild steel substrate was severely degraded due to exposure to 1.0 M HCl, as shown in Fig. 11. However, the substrate's surface became smoother and less

**Table 9**

Lists the percent Mass of the various elements determined by EDX study of the substrate steel in 1.0 M HCl absent and present Q-Cl and Q-H at 298 K.

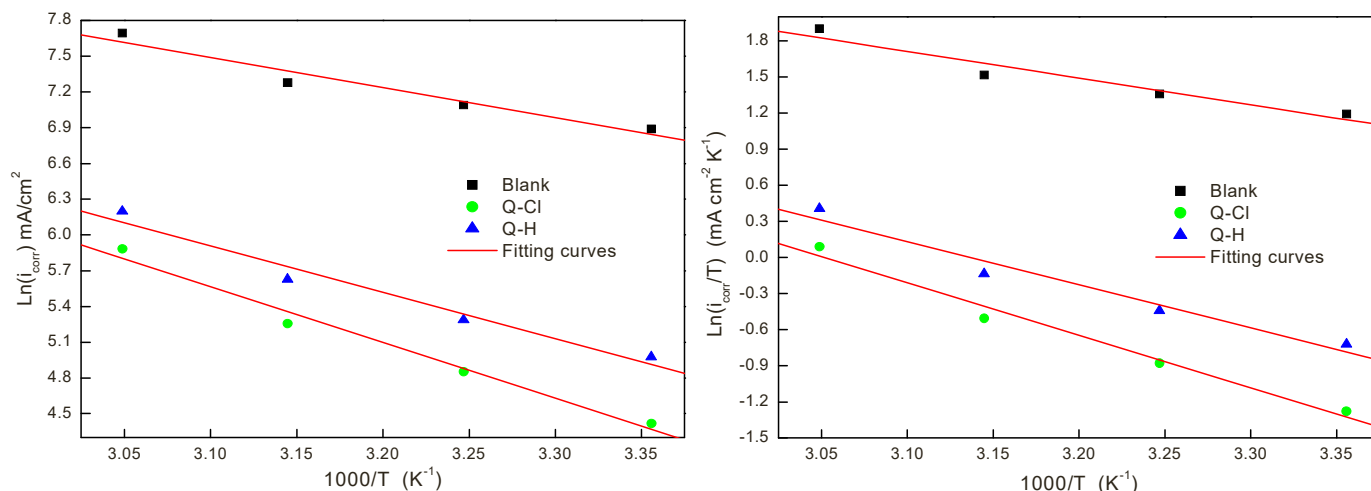| Elements | % Mass of steel in Blank solution | % Mass of steel in blank solution with Q-Cl | % Mass of steel in blank solution with Q-H |
|---|---|---|---|
| **C** | 2.91 | 3.2 | 3.6 |
| **O** | 25.91 | 2.1 | 10.9 |
| **Si** | 0.35 | – | – |
| **Cl** | 1.04 | – | – |
| **N** | – | 0.8 | 0.6 |
| **Fe** | 69.79 | 93.9 | 84.9 |



**Fig. 10.** Arrhenius plots for mild steel corrosion in 1 M HCl in the absence and in presence of $10^{-3}$ M of Q-Cl and Q-H.
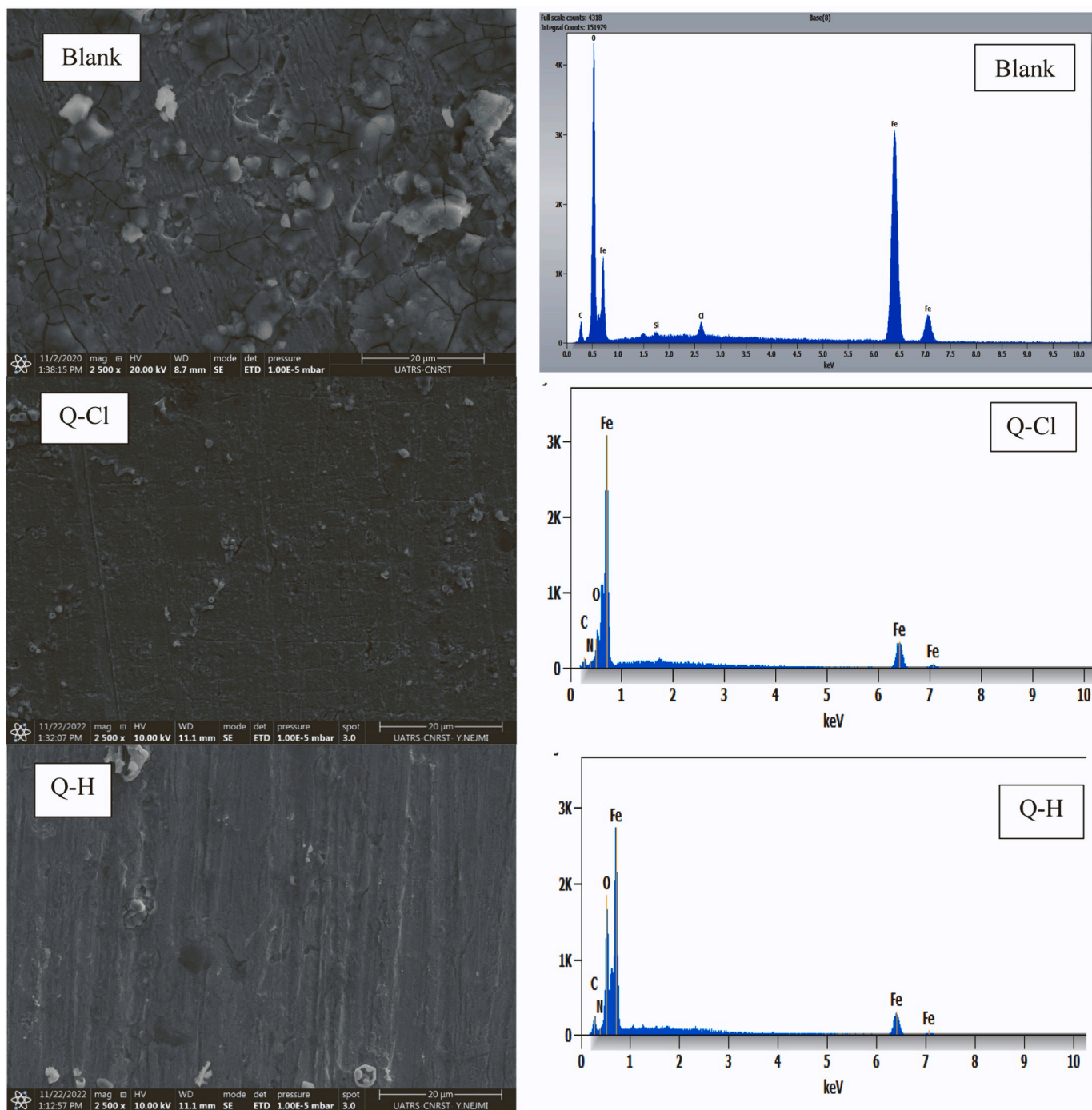
**Fig. 11.** A mild steel surface was examined using SEM microscopy and EDX spectra before and after 6 hours of immersed in 1.0 M HCl present and absent Q-Cl and Q-H at 298 K.

porous when immersed in an aggressive solution containing $10^{-3}$ M of Q-Cl and Q-H inhibitors. This enhancement can be attributed to the formation of a thicker protective layer on the substrate's surface, which offers improved corrosion protection. Overall, our findings suggest that the adsorption of Q-Cl and Q-H inhibitors enhances the mild steel substrate's resistance to corrosion by forming a protective layer. These insights provide valuable understanding of corrosion inhibition mechanisms and have potential implications for the development of novel corrosion inhibitors in the future.

The obtained spectra are illustrated in Fig. 11, and Table 9 provides information on the weight percentages of different elements adsorbed on the steel surface. The peak for iron (Fe) and oxygen (O) in the blank

spectra in Fig. 11 indicates the formation of iron oxide/hydroxide on the steel sample's surface. However, when the inhibited specimens (with Q-Cl and Q-H) were examined, a reduced percentage of oxygen was detected. This suggests that Q-Cl and Q-H significantly reduce iron oxide formation, making them effective inhibitors of mild steel corrosion. The proportions of the different components identified on the mild steel surface are reported in Table 9. The presence of the distinctive nitrogen (N) peak in Fig. 11 and the percentage of N (0.8 % for Q-Cl and 0.6 % for Q-H) in Table 9 demonstrates adsorption on the mild steel. Furthermore, the adsorption on mild steel is further evidenced by the presence of the characteristic nitrogen (N) peak in Fig. 11 and the percentage of N (0.8 % for Q-Cl and 0.6 % for Q-H) reported in Table 9.

## 3.5. Inductively coupled plasma (ICP) spectrometry

ICP spectrometry was used to examine the elemental composition and concentration of dissolved iron ions in both inhibited and uninhibited solutions. Table 10 presents the acquired $Fe^{2+}$ ion concentrations as well as the inhibitory effectiveness following a 6-hour immersion. As shown in Table 10, the concentration of $Fe^{2+}$ ions decreased with an increase in the concentration of the two investigated inhibitors. Specifically, the concentration of $Fe^{2+}$ ions was 328.9 mg/L in the control group, 25.8 mg/L in the Q-Cl group, and 53.4 mg/L in the Q-H group. The effectiveness ($\eta ICP\%$) also increased with the reduction in the concentration of $Fe^{2+}$ ions in the inhibited solution. These findings imply that steel dissolution is effectively prevented in the presence of the examined inhibitors. Therefore, our data suggest that Q-Cl and Q-H inhibitors have a significant inhibitory impact on steel corrosion in acidic conditions. The results of our study could be useful in the development of innovative corrosion inhibitors for mild steel in HCl solution.

## 3.6. DFT calculations

### 3.6.1. Prediction of the major microspecies

In an acidic medium, inhibitor molecules have the ability to undergo protonation. In this study, the consideration was given to only the most protonated species of the studied inhibitors to accurately simulate the experimental conditions. To identify the most likely forms of protonation in acidic media, calculations were conducted to determine the distribution of microspecies as a function of pH (ranging from 0 to 14) for the studied derivatives. This analysis allowed us to assess the relative abundance of different protonation states and select the most probable forms of protonation for the inhibitors under consideration. The selection of the most stable forms was carried out using the MarvinSketch software [45]. Fig. 12 displays the analysis of the existing forms of the Q-Cl and Q-H at different pH levels using the Marvinsketch program. The optimized structures of the most stable forms are superimposed in Fig. 12.

#### 3.6.1.1. DFT descriptors.
One crucial aspect is examining the electron distribution within the highest occupied molecular orbital (HOMO) and lowest unoccupied molecular orbital (LUMO). In this context, frontier molecular orbital (FMO) studies provide insights into the interaction mechanism between the organic inhibitor molecule and the Fe surface. Fig. 13 shows the optimized molecular structures of Q-Cl and Q-H. Frontier molecular orbitals and HOMO–LUMO energy gaps of Q-Cl and Q-H in their protonated form were calculated using the B3LYP/6–311G (d,p) level of theory in aqueous solution. The quantum chemical descriptors were computed and summarized in Table 11. After optimizing the molecular geometry of the studied molecules, it was revealed that both the benzimidazole and quinazolinone rings exhibited a planar orientation. This planar conformation renders them highly suitable for adsorption onto metal surfaces. The planar structure facilitates a larger contact surface area and promotes better interaction with the metal

substrate, thus favoring their adsorption and potentially enhancing their inhibitory properties.

Moreover, the analysis of the electron density distributions in the HOMO and LUMO of the studied inhibitors reveals that electron density is evenly distributed throughout the entire molecular framework. This characteristic indicates a similarity in the donor-acceptor capacity of the molecules. The chlorine atom in Q-Cl serves as an electron donor, which can contribute to its higher inhibitory capacity compared to the Q-H molecule. Moreover, the HOMO state indicates the molecule's potential to donate electrons, while the LUMO state indicates its ability to accept electrons. We can therefore deduce that the capacity of an inhibitory molecule to donate electrons increases as its $E_{HOMO}$ values increase, while its propensity to accept electrons increases as its $E_{LUMO}$ values decrease [46]. Further analysis of Fig. 14, it is evident that the Q-Cl molecule exhibits a significantly lower $\Delta E$ value (4.516 eV), indicating a higher degree of chemical reactivity when compared to Q-H (4.530 eV).

Several other electronic properties were determined and discussed, including softness ($\sigma$) and hardness ($\eta$) values, the global electrophilicity ($\omega$), the back-donation energy ($\Delta E_{b-d}$), and the fraction of transferred electrons ($\Delta N$). These properties provide valuable insights into the reactivity and stability of the inhibitor molecules and contribute to a comprehensive understanding of their inhibitory effects. These descriptors were estimated with the following Equations [47,48]:

$$\Delta E_{gap} = E_{LUMO} - E_{HOMO} \tag{12}$$

$$\chi = \frac{-(E_{LUMO} - E_{HOMO})}{2} \tag{13}$$

$$\eta = \frac{E_{LUMO} - E_{HOMO}}{2} \tag{14}$$

$$\sigma = \frac{1}{\eta} \tag{15}$$

$$\omega = \left(\frac{\chi^2}{2\eta}\right) \tag{16}$$

$$\Delta E_{b-d} = -\frac{\eta}{4} \tag{17}$$

$$\Delta N = \frac{\varphi_{Fe} - \chi_{inh}}{2(\eta_{Fe} + \eta_{inh})} \tag{18}$$

The terms $\varphi_{Fe}$ and $\eta_{Fe}$ correspond to the "work function" and absolute hardness of iron (Fe) metal, with values specified as 4.82 eV and 0 eV, respectively. In contrast, $\chi_{inh}$ and $\eta_{inh}$ denote the electronegativity and hardness parameters of the inhibitor, respectively [49].

#### 3.6.1.2. Haut du formulaire.
Higher softness and lower hardness indicate a greater tendency for inhibitor molecules to interact with metals. These properties influence the molecular behavior and binding affinity with metal surfaces, and hence the inhibitory properties of the studied compounds [50]. Moreover, the global electrophilicity value ($\omega$) sheds light on the electron-accepting capacity of inhibitor compounds. Since $\triangle E_{b-d} < 0$, the charge transfer to donate electrons from the inhibitor is energetically advantageous, and these electrons are then back-donated in the opposite direction, according to the electron back donation ($\triangle E_{b-d}$) indicator [51].

The value of $\Delta N$ is positive, which indicates the transfer of electrons from the studied molecules to the Fe surface. Also, Q-H and Q-Cl show $\Delta N$ values below 3.6 (Table 11), indicating that electrons are transferred from the inhibitor molecules to the iron surface. This electron transfer facilitates the formation of coordination bonds and promotes the development of a protective layer against corrosion [52]. In this study, the trend of inhibition observed in the studied compounds (Q-Cl>Q-H) aligns with their electronic properties presented in Table 9.

**Table 10**
Concentration of iron ions in 1.0 M HCl with and without different concentrations of Q-Cl and Q-H after 6 h immersion.

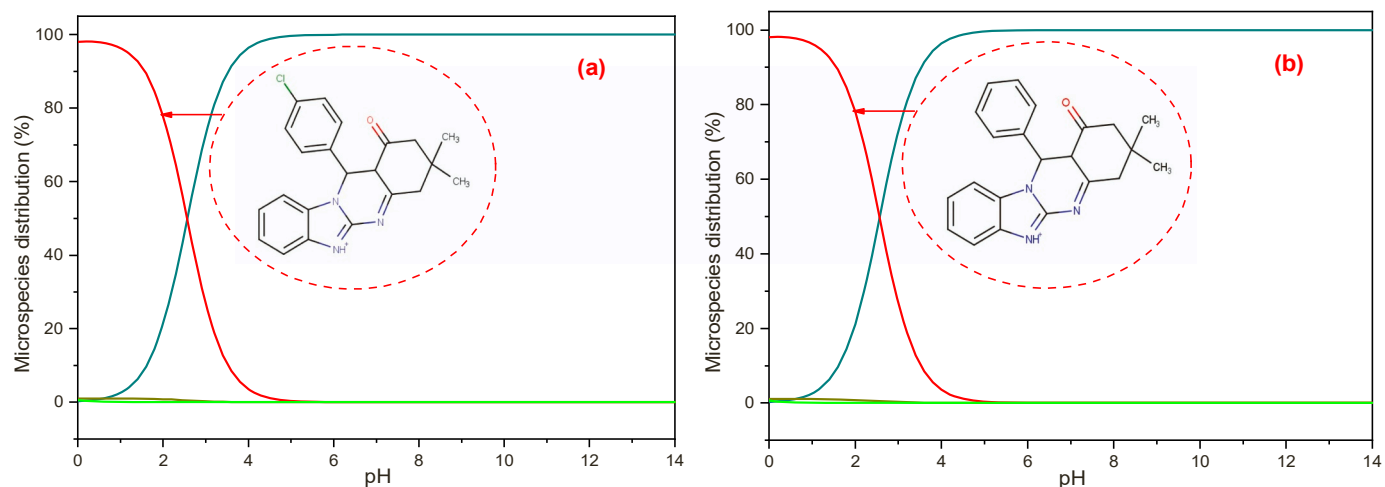| Medium | Conc. M | Conc. of $Fe^{2+}$ ions mg/L | $\eta_{ICP}\%$ |
|---|---|---|---|
| *1.0 M HCl* | – | 328.9 | – |
| Q-Cl | $10^{-6}$ | 58.9 | 82.1 |
| | $10^{-5}$ | 52.7 | 83.9 |
| | $10^{-4}$ | 38.4 | 88.3 |
| | $10^{-3}$ | 25.8 | 92.1 |
| Q-H | $10^{-6}$ | 100.4 | 69.4 |
| | $10^{-5}$ | 82.6 | 74.9 |
| | $10^{-4}$ | 71.5 | 78.2 |
| | $10^{-3}$ | 53.4 | 83.7 |

**Fig. 12.** Percentage of distribution of different forms of (a) Q-Cl and (b) Q-H as a function of pH obtained by the Marvinsketch Software.
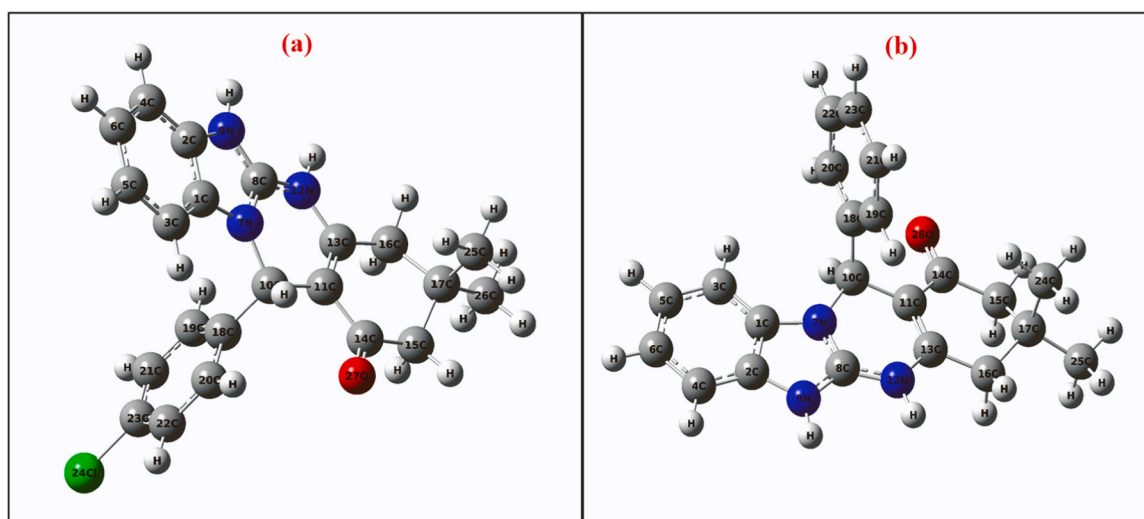


**Fig. 13.** Optimised geometry of (a) Q-Cl and (b) Q-H in their protonated form in aqueous solution.

**Table 11**

Quantum molecular descriptors for investigated inhibitor molecules aqueous phase.

| Molecule | $E_{HOMO}$ (eV) | $E_{LUMO}$ (eV) | $\Delta E_{gap}$ (eV) | $\eta$ (eV) | $s$ ($eV^{-1}$) | $\Delta E_{b-d}$ (eV) | $\chi$ (eV) | $\omega$ | $\Delta N$ |
|---|---|---|---|---|---|---|---|---|---|
| Q-Cl | −6.797 | −2.281 | 4.516 | 2.258 | 0.442 | −0.564 | 4.539 | 4.562 | 0.062 |
| Q-H | −6.780 | −2.249 | 4.530 | 2.265 | 0.441 | −0.566 | 4.5152 | 4.499 | 0.067 |

*3.6.1.3. Local reactivity.* The Fukui indices (FI) are commonly used to assess the local chemical reactivity of an inhibitor compound [53]. This analysis helps identify atoms within the molecule susceptible to electrophilic and nucleophilic attacks. To calculate the Fukui indices, the electronic population parameters of the atom in the neutral system ($\rho N$) and the charged systems, namely anionic ($\rho(N-1)$) and cationic ($\rho(N+1)$), are utilized:

$$f_N^+(r) = \rho_{(N+1)}(r) - \rho_N(r) \qquad (19)$$

$$f_N^-(r) = \rho_N(r) - \rho_{(N-1)}(r) \qquad (20)$$

A positive Fukui function ($f_N^+$) at a particular center indicates a propensity for nucleophilic attacks. On the other hand, a negative Fukui function ($f_N^-$) implies a preference for electrophilic attacks. The values of the Fukui indices for the protonated forms of Q-Cl and Q-H were

calculated and presented in Fig. 15. These parameters were used to determine the atomic centers within the molecules that are susceptible to nucleophilic or electrophilic attacks.

According to the Fig. 15, for both molecules, the regions corresponding to the benzimidazole and quinazolinone rings are characterized by a dual electrophilic/nucleophilic property. In addition, in the Q-H molecule, the oxygen atom O26 ($f_N^+$= 0.0614 and $f_N^-$= 0.0971), and in the Q-Cl molecule, O27 ($f_N^+$ = 0.0583 and $f_N^-$= 0.0971) and Cl24 ($f_N^+$= 0.0240 and $f_N^-$= 0.0146) are also characterized by significant values of the Fukui indices. Furthermore, it can be also observed that these locations are highly consistent with the full distribution of HOMO and LUMO along the Q-H and Q-Cl structures.
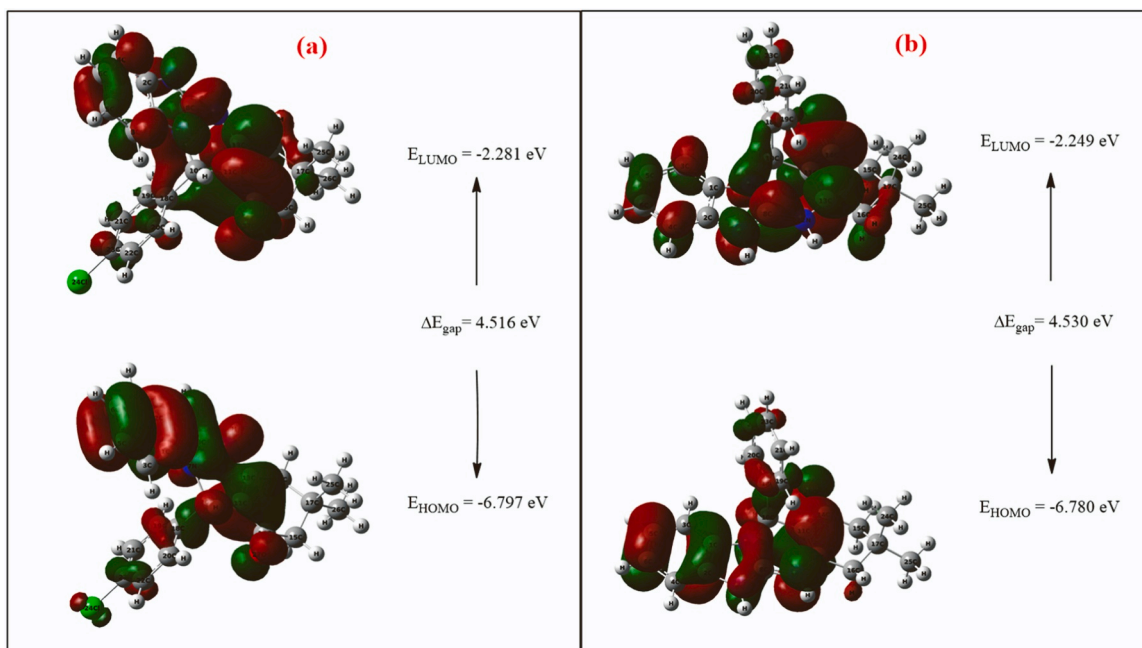
**Fig. 14.** Frontier molecular orbitals and HOMO–LUMO energy gaps of (a) Q-Cl and (b) Q-H in their protonated form in aqueous solution.
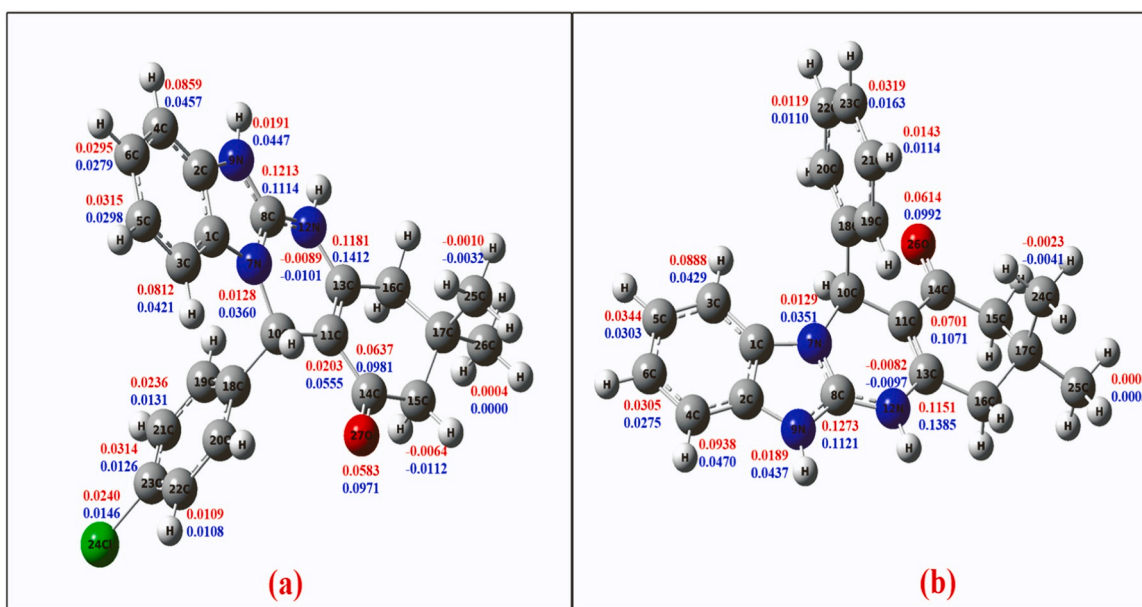


**Fig. 15.** Graphical representation of the Fukui function indices for (a) Q-Cl and (b) Q-H inhibitors in their protonated forms in aqueous solution.

## 4. Conclusion

This study investigates the effectiveness of quinazoline compounds in reducing steel corrosion in a 1.0 M hydrochloric acid (HCl) solution. By employing polarization curves and Electrochemical Impedance Spectroscopy (EIS), we determined that these compounds exhibit significant mixed-type inhibition properties. Specifically, the inhibition efficiency follows the order Q-Cl > Q-H. This finding is corroborated by morphological analyses, which confirm that the inhibitors successfully mitigate both anodic dissolution and cathodic hydrogen gas evolution in HCl solutions. The Langmuir adsorption model effectively describes the adsorption behavior of the inhibitors, with thermodynamic parameters suggesting that the adsorption process is predominantly chemical. Additionally, analysis of the electron density distribution reveals that the structure of the inhibitors plays a crucial role in their adsorption onto the metal surface. Calculations of Density Functional Theory (DFT) descriptors further support the observed trend in corrosion inhibition efficiency, highlighting Q-Cl's superior performance compared to Q-H.

## CRediT authorship contribution statement

**Zakia Aribou:** Writing - original draft. **Moussa Ouakki:** Writing – original draft, Visualization, Supervision, Software. **Fatima El Hajri:** Formal analysis, Data curation. **Elhachmia Ech-chihbi:** Software, Methodology. **Issam Saber:** Formal analysis, Data curation. **Zakaria Benzekri:** Supervision, Methodology. **Said Boukhris:** Visualization, Validation. **Mohammad K. Al-Sadoon:** Writing – original draft. **Mouhsine Galai:** Visualization, Software. **Charafeddine Jama:** Writing

– original draft. **Mohamed Ebn Touhami:** Writing – original draft, Validation, Supervision.

## Declaration of Competing Interest

The authors declare that they have no known competing financial interests or personal relationships that could have appeared to influence the work reported in this paper.

## Acknowledgements

## References

[1] A.Ghany F. Shoair, M.M. Motawea, A.S.A. Almalki, M.A.H. Shanab, A. El-Basiony, H.A. Nasef, Expired terazosin as environmentally safe corrosion inhibitor for 1018 carbon steel in 1 M HCl solution: Experimental and computational studies, International Journal of Electrochemical Science, https://doi.org/10.1016/j.ijoes.2023.100397.

[2] D. Xia, C. Deng, D. Macdonald, S. Jamali, D. Mills, J. Luo, M.G. Strebl, M. Amiri, W. Jin, S. Song, W. Hu, Electrochemical measurements used for assessment of corrosion and protection of metallic materials in the field: A critical review, Journal of Materials Science & Technology, https://doi.org/10.1016/j.jmst.2021.11.004.

[3] M. Abdallah, H.M. Al-Tass, B.A. AL Jahdaly, A.S. Fouda. Inhibition properties and adsorption behavior of 5-arylazothiazole derivatives on 1018 carbon steel in 0.5 M H2SO4 solution, Journal of Molecular Liquids, https://doi.org/10.1016/j.molliq.2016.01.077.

[4] M.A. Bedair, S.A. Soliman, M.F. Bakr, E.S. Gad, H. Lgaz, I.-Min Chung, M. Salama, F.Z. Alqahtany. Benzidine-based Schiff base compounds for employing as corrosion inhibitors for carbon steel in 1.0 M HCl aqueous media by chemical, electrochemical and computational methods. Journal of Molecular Liquids, https://doi.org/10.1016/j.molliq.2020.114015.

[5] W.M.K.W.M. Ikhmal, M.F.M. Maria, W.A.W. Rafizah, W.N.W.M. Norsani, M.G.M. Sabri, Corrosion inhibition of mild steel in seawater through green approach using Leucaena leucocephala leaves extract, International Journal of Corrosion and Scale Inhibition, doi: 10.17675/2305-6894-2019-8-3-12.

[6] Z. Aribou, N. Khemmoua, R.A. Belakhmima, I. Chaouki, M. EbnTouhami, R. Touir, S. Bakkali, Effect of polymer additive on structural and morphological properties of Cu-electrodeposition from an acid sulfate electrolyte: experimental and theoretical studies, Journal of Electroanalytical Chemistry. https://doi.org/10.1016/j.jelechem.2023.117722.

[7] P.B. Raja, M.G. Sethuraman. Natural products as corrosion inhibitor for metals in corrosive media — a review. Materials Letters, https://doi.org/10.1016/j.matlet.2007.04.079.

[8] A. Al-Amiery, F. Binti Kassim, A. Kadhum, et al. Synthesis and characterization of a novel eco-friendly corrosion inhibition for mild steel in 1 M hydrochloric acid. Scientific Reports. https://doi.org/10.1038/srep19890.

[9] A. Kosari, M. Momeni, R. Parvizi, M. Zakeri, M.H. Moayed, A. Davoodi, H. Eshghi, Theoretical and electrochemical assessment of inhibitive behavior of some thiophenol derivatives on mild steel in HCl, Corrosion Science, https://doi.org/10.1016/j.corsci.2011.05.009.

[10] A. Kosari, M.H. Moayed, A. Davoodi, R. Parvizi, M. Momeni, H. Eshghi, H. Moradi, Electrochemical and quantum chemical assessment of two organic compounds from pyridine derivatives as corrosion inhibitors for mild steel in HCl solution under stagnant condition and hydrodynamic flow, Corrosion Science, https://doi.org/10.1016/j.corsci.2013.09.009.

[11] Z. Aribou, M. Ouakki, N. Khemmou, S. Sibous, E. Echchihbi, O. Kharbouch, M. Galai, S. Boukhris, A.A. AlObaid, I. Warad, M.Ebn Touhami. Detailed experimental of indazole derivatives as corrosion inhibitor for brass in acidic environment: electrochemical/theoretical/surface studies. Journal of Applied Electrochemistry, https://doi.org/10.1007/s10800-023-01960-6.

[12] Z. Aribou, M. Ouakki, N. Khemmou, S. Sibous, E. Echchihbi, Z. Benzekri, M. Galai, A. Souizi, S. Boukhris, M.Ebn Touhami, A.A. AlObaid, I. Warad, Exploring the adsorption and corrosion inhibition properties of indazole as a corrosion inhibitor for brass alloy in HCl medium: a theoretical and experimental study, Materials Today Communications, https://doi.org/10.1016/j.mtcomm.2023.107061.

[13] B.P. Markhali, R. Naderi, M. Mahdavian, M. Sayebani, S.Y. Arman, Electrochemical impedance spectroscopy and electrochemical noise measurements as tools to evaluate corrosion inhibition of azole compounds on stainless steel in acidic media, Corrosion Science, https://doi.org/10.1016/j.corsci.2013.06.010.

[14] M.El Faydy, F. Benhiba, M. Alfakeer, A.Mohsen Al-bonayan, N. Timoudan, I. Warad, B. Lakhrissi, M. Abdallah and A. Zarrouk, Corrosion Resistance of Two Newly Synthesized 8-Quinolinol-Benzimidazoles on Carbon Steel: An Experimental and Theoretical Investigation, Journal of Materials Engineering and Performance, https://doi.org/10.1007/s11665-023-08919-w.

[15] A.S. El-Tabei, M.A. Hegazy, A corrosion inhibition study of a novel synthesized gemini nonionic surfactant for carbon steel in 1 M HCl solution, J. Surfactants Deterg., https://doi.org/10.1007/s11743-013-1457-1.

[16] J.O. Mendes, E.C. da Silva, A.B. Rocha, On the nature of inhibition performance of imidazole on iron surface, Corrosion Science https://doi.org/10.1016/j.corsci.2011.12.011.

[17] A.S. Fouda, A.M. El-desoky, Hala M. Hassan, Quinazoline Derivatives as Green Corrosion Inhibitors for Carbon Steel in Hydrochloric Acid Solution"s, International Journal of Electrochemical Science, https://doi.org/10.1016/S1452-3981(23)14728-6.

[18] N. Errahmany, M. Rbaa, A.S. Abousalem, A. Tazouti, M. Galai, E.El Kafssaoui, M. Ebn Touhami, B. Lakhrissi, R. Touir, Experimental, DFT calculations and MC simulations concept of novel quinazolinone derivatives as corrosion inhibitor for mild steel in 1.0 M HCl medium, Journal of Molecular Liquids, https://doi.org/10.1016/j.molliq.2020.113413.

[19] M.J. Frisch, G.W. Trucks, H.B. Schlegel, G.E. Scuseria, M.A. Robb, J.R. Cheeseman, G. Scalmani, V. Barone, B. Mennucci, et al., Gaussian 09W, Revision D.01, Gaussian, Inc, Wallingford CT, 2013.

[20] C. Lee, W. Yang, R.G. Parr, Development of the Colle-Salvetti correlation-energy formula into a functional of the electron density, Phys. Rev. B 37 (1988) 785–789, https://doi.org/10.1103/PhysRevB.37.785.

[21] M.I. AlBeladi, Y. Riadi, M.H. Geesi, O. Ouerghi, E. Anouar, A. Kaiba, A.H. Alamri, T.A. Aljohani, "Benzalkonium chloride/titanium dioxide as an effective corrosion inhibitor for carbon steel in a sulfuric acid solution", Journal of Saudi Chemical Society, https://doi.org/10.1016/j.jscs.2022.101481.

[22] K.F. Khaled, Application of electrochemical frequency modulation for monitoring corrosion and corrosion inhibition of iron by some indole derivatives in molar hydrochloric acid. Materials Chemistry and Physics, https://doi.org/10.1016/j.matchemphys.2008.05.056.

[23] N.S. Abdelshafi, M.A. Sadik, Madiha A. Shoeib, Shimaa Abdel Halim Corrosion inhibition of aluminum in 1 M HCl by novel pyrimidine derivatives, EFM measurements, DFT calculations and MD simulation. Journal of Saudi Chemical Society, https://doi.org/10.1016/j.arabjc.2021.103459.

[24] K. Shalabi, Y.M. Abdallah, A.S. Fouda, Corrosion inhibition of aluminum in 0.5 M HCl solutions containing phenyl sulfonylacetophenoneazo derivatives, Research on Chemical Intermediates, https://doi.org/10.1007/s11164-014-1561-5.

[25] A.S. Fouda, Ali H. El-Azaly, R.S. Awad, A.M. Ahmed New Benzonitrile Azo Dyes as Corrosion Inhibitors for Carbon Steel in Hydrochloric Acid Solutions. International Journal of Electrochemical Science, https://doi.org/10.1016/S1452-3981(23)07782-9.

[26] Li Huang, Ying Liu, Zi-Ming Wang, Wen-Yu Lu, Xin-Yue Li, Hui-Jing Li, Yan-Chao Wu, Exploration of procyanidin C1 from Uncaria laevigata as a green corrosion inhibitor in industry: Electrochemical assessment, theoretical simulation, and environmental safety, Separation and Purification Technology, https://doi.org/10.1016/j.seppur.2023.123950.

[27] H. Chahmout, M. Ouakki, S. Sibous, M. Galai, N. Arrousse, E. Ech-chihbi, Z. Benzekri, S. Boukhris, A. Souizi, M. Cherkaoui, New pyrazole compounds as a corrosion inhibitor of stainless steel in 2.0 M H2SO4 medium: Electrochemical and theoretical insights, Inorganic Chemistry Communications, https://doi.org/10.1016/j.inoche.2022.110150.

[28] J. Haque, Mohammad F.R. Zulkifli, N. Ismail, M.A. Quraishi, M. Sabri, M. Ghazali, E. Berdimurodov, and W.M.N. Bin Wan Nik. Environmentally Benign Water-Soluble Sodium L-2-(1-Imidazolyl) Alkanoic Acids as New Corrosion Inhibitors for Mild Steel in Artificial Seawater. ACS Omega, https://doi.org/10.1021/acsomega.3c00366.

[29] M. Ouakki, Z. Aribou, K. Dahmani, I. Saber, M. Galai, B. Srhir, M. Cherkaoui, C. Verma. Book Title: Phytochemistry in Corrosion Science Chapter: Natural Polymers and their Derivatives as Corrosion Inhibitors. Taylor & Francis Group 2024. DOI: 10.1201/9781003394631-5.

[30] F. Benhiba, Z. Benzekri, Y. Kerroum, N. Timoudan, R. Hsissou, A. Guenbour, M. Belfaquir, S. Boukhri, A. Bellaouchou, H. Oudda, A. Zarrouk, Assessment of inhibitory behavior of ethyl 5-cyano-4-(furan-2-yl)-2-methyl-6-oxo-1,4,5,6-tetra-hydropyridine-3-carboxylate as a corrosion inhibitor for carbon steel in molar HCl: Theoretical approaches and experimental investigation, Journal of the Indian Chemical Society https://doi.org/10.1016/j.jics.2023.100916.

[31] D.Q. Huong, N.T. Lan Huong, T.T. Anh Nguyet, T. Duong, D. Tuan, N.M. Thong, P.C. Nam. Pivotal Role of Heteroatoms in Improving the Corrosion Inhibition Ability of Thiourea Derivatives. ACS Omega. https://doi.org/10.1021/acsomega.0c04241.

[32] H. Yu, C. Li, B. Yuan, L. Li, C. Wang. The inhibitive effects of AC-treated mixed self-assembled monolayers on copper corrosion. Corrosion Science, doi:10.1016/j.corsci.2017.03.0.

[33] Z.S. Mousavi, S. Karimi, A. Heidarpour, S.M. Hosseini, S. Ghasemi, Microstructural variation and corrosion behavior of 60/40 Brass/Ti2SC surface composite through friction stir processing, J. Mater. Eng. Perform. (2022) 1–12, https://doi.org/10.1007/s11665-021-06441-5.

[34] M. Galai, M. Rbaa, M. Ouakki, K. Dahmani, S. Kaya, N. Arrousse, M. Ebn Touhami. Functionalization effect on the corrosion inhibition of novel eco-friendly compounds based on 8-hydroxyquinoline derivatives: Experimental, theoretical and surface treatment. Chemical Physics Letters, https://doi.org/10.1016/j.cplett.2021.138700.

[35] J. Lazrak, E. Ech-chihbi, R. Salim, T. Saffaj, Z. Rais, M. Taleb, Insight into the corrosion inhibition mechanism and adsorption behavior of aldehyde derivatives for mild steel in 1.0 M HCl and 0.5 M H2SO4, Colloids and Surfaces A: Physicochemical and Engineering Aspects, https://doi.org/10.1016/j.colsurfa.2023.131148.

[36] G. Weinan, X. Bin, Y. Xiaoshuang, L. Ying, C. Yun, Y. Wenzhong; Halogen-substituted thiazole derivatives as corrosion inhibitors for mild steel in 0.5 M sulfuric acid at high temperature, Journal of the Taiwan Institute of Chemical Engineers, https://doi.org/10.1016/j.jtice.2019.02.018.

[37] L. Baoyi, L. Guo, X. i Bai, S. Zhang, Z. Zhang, H. Zhou, H. Dong, Y. Li, Experimental and theoretical investigation of 1-Hexyl-3-methylimidazolium iodide as a corrosion inhibitor for mild steel in HCl environment, International Journal of Electrochemical Science, https://doi.org/10.1016/j.ijoes.2024.100580.

[38] H. Chahmout, M. Ouakki, S. Sibous, M. Galai, N. Arrousse, E. Ech-chihbi, Z. Benzekri, S. Boukhris, A. Souizi, M. Cherkaoui, New pyrazole compounds as a corrosion inhibitor of stainless steel in 2.0 M $H_2SO_4$ medium: Electrochemical and theoretical insights, Inorganic Chemistry Communications, https://doi.org/10.1016/j.inoche.2022.110150.

[39] H. Lgaz, K. Toumiat, S. Jodeh, R. Salghi. Inhibition of Mild Steel Corrosion in 1 M HCl Medium by Tangeretin, Applied Journal of Environmental Engineering Science, https://doi.org/10.48422/IMIST.PRSM/ajees-v2i2.7103.

[40] K. Mzioud, A. Habsaoui, M. Ouakki, M. Galai, S. El Fartah, M. Ebn Touhami. Inhibition of copper corrosion by the essential oil of Allium sativum in 0.5 M H2SO4 solutions. SN Applied Sciences. https://doi.org/10.1007/s42452-020-03393-8.

[41] H. Ouici, M. Tourabi, O. Benali, C. Selles, C. Jama, A. Zarrouk, F. Bentiss. Adsorption and corrosion inhibition properties of 5-amino 1,3,4-thiadiazole-2-thiol on the mild steel in hydrochloric acid medium: Thermodynamic, surface and electrochemical studies. Journal of Electroanalytical Chemistry, https://doi.org/10.1016/j.jelechem.2017.09.018.

[42] M. Galai, M. Rbaa, H. Serrar, M. Ouakki, A. Ech-chebab, Ashraf S. Abousalem, E. Ech-chihbi, K. Dahmani, S. Boukhris, A. Zarrouk, M. Ebn Touhami. S-Thiazine as effective inhibitor of mild steel corrosion in HCl solution: Synthesis, experimental, theoretical and surface assessment. Colloids and Surfaces A: Physicochemical and Engineering Aspects, https://doi.org/10.1016/j.colsurfa.2020.126127.

[43] M. Bouklah, N. Benchat, B. Hammouti, A. Aouniti, S. Kertit. Thermodynamic characterisation of steel corrosion and inhibitor adsorption of pyridazine compounds in 0.5 M H2SO4. Materials Letters, https://doi.org/10.1016/j.matlet.2005.12.051.

[44] M. Galai, M. Rbaa, M. Ouakki, A.S. Abousalem, E. Ech-chihbi, K. Dahmani, M. Ebn Touhami. Chemically functionalized of 8-hydroxyquinoline derivatives as efficient corrosion inhibition for Steel in 1.0 M HCl solution: Experimental and Theoretical studies. Surfaces and Interfaces, https://doi.org/10.1016/j.molstruc.2022.132784.

[45] MarvinSketch Software, Version 18.22, ChemAxon Ltd., (2018).

[46] H. Assad, S. Kumar, S.Kr Saha, N. Kang, I. Fatma, H. Dahiya, P.K. Sharma, A. Thakur, S. Sharma, R. Ganjoo, A. Kumar, Evaluating the adsorption and corrosion inhibition capabilities of Pyridinium - P - Toluene Sulphonate on MS in 1 M HCl medium: An experimental and theoretical study, Inorganic Chemistry Communications https://doi.org/10.1016/j.inoche.2023.110817.

[47] R. Kerkour, N. Chafai, O. Moumeni, S. Chafaa, Novel α-aminophosphonate derivates synthesis, theoretical calculation, Molecular docking, and in silico prediction of potential inhibition of SARS-CoV-2, Journal of Molecular Structure, https://doi.org/10.1016/j.molstruc.2022.134196.

[48] M. Ouakki, M. Galai, M. Rbaa, A.S. Abousalem, B. Lakhrissi, M.Ebn Touhami, M. Cherkaoui, Electrochemical, thermodynamic and theoretical studies of some imidazole derivatives compounds as acid corrosion inhibitors for mild steel, Journal of Molecular Liquids, https://doi.org/10.1016/j.molliq.2020.114063.

[49] J. Lazrak, E. Ech-chihbi, B. El Ibrahimi, F. El Hajjaji, Z. Rais, M. Tachihante, M. Taleb, Detailed DFT/MD simulation, surface analysis and electrochemical computer explorations of aldehyde derivatives for mild steel in 1.0 M HCl, Colloids and Surfaces A: Physicochemical and Engineering Aspects, https://doi.org/10.1016/j.colsurfa.2021.127822.

[50] A. Bouoidina, E. Ech-chihbi, F. El-Hajjaji, B. El Ibrahimi, S. Kaya, M. Taleb, Anisole derivatives as sustainable-green inhibitors for mild steel corrosion in 1M HCl: DFT and molecular dynamic simulations approach Journal of Molecular Liquids, https://doi.org/10.1016/j.molliq.2020.115088.

[51] B.T. Ogunyemia, D.F. Latonab, A.A. Ayindec, I.A. Adejoro, Theoretical Investigation to Corrosion Inhibition Efficiency of Some Chloroquine Derivatives Using Density Functional Theory, Advanced Journal of Chemistry-Section A, https://doi.org/10.33945/SAMI/AJCA.2020.4.10.

[52] O. Dagdag, Z. Safi, Y. Qiang, H. Erramli, L. Guo, C. Verma, E.E. Ebenso, A. Kabir, N. Wazzan, A. El Harfi, Synthesis of macromolecular aromatic epoxy resins as anticorrosive materials: computational modeling reinforced experimental studies, ACS Omega, https://doi.org/10.1021/acsomega.9b02678.

[53] E. Ech-chihbi, A. Nahlé, R. Salim, F. Benhiba, A. Moussaif, F. El-Hajjaji, A. Zarrouk, Computational, MD simulation, SEM/EDX and experimental studies for understanding adsorption of benzimidazole derivatives as corrosion inhibitors in 1.0 M HCl solution. Journal of Alloys and Compounds, https://doi.org/10.1016/j.jallcom.2020.155842 ·